Assessment of Pu and MA utilisation in deep burn Prismatic HTR by Monte Carlo Method - MCB

Appendix A

Deliverable 124

Work Package 1

Project PUMA

Jerzy Cetnar
Mariusz Kopeć
Mikołaj Oettingen

AGH-UST Krakow, Poland

Contents

List of Figures

List of Tables

Scope

This report describes the work done under the scope of deliverable 124 for the PuMA project, which is part of the European Commission's 6th framework program. It is concern with application of Monte Carlo burnup calculation system – MCB for analysis of reactor physics and core design of prismatic HTR for plutonium and MA utilisation in deep burn mode.

1. Introduction

As some features of various nuclear reactors are similar, the other differs thus requiring an additional attention. The core of an HTR reactor is characterized by specific features, which imposes particular requirements on analytical tools and models that are to be used for analysis of its physics and safety along with fuel cycle analysis. The major differences, as compared to other systems like LWR or FBR, that need to be taken into consideration in analysis of nuclear transmutation in deep burn mode are concerned with high temperature of the fuel, different fuel form and different moderator. These specific features are:

- high operational temperature of the fuel and graphite, which necessitates the thermal-hydraulic and neutronic coupling;
- high level of core heterogeneity caused by a fine structure of fuel compacts filled with TRISO particles, for which a highly structured geometrical model is needed in order to account for neutron spectra effects that occur in the fuel due to resonant cross sections;
- deep neutron thermalisation, which imposes few important neutronic effects like: shortening free path length, higher flux gradients, stronger influence of reflectors, and as a consequence needed attention for spatial effects particularly in the vicinity of control rods or reflectors;
- large core size in terms of free path length as well as of the core fine structure length (i.e. TRISSO kernel size), which is primarily caused by relatively low average power density.

Due to the existing complexity of burnup process, it is effective to apply an integrated calculation system, which will allow the user taking into consideration the spatial effects of full heterogeneous reactor model with continuous energy representation of cross section and the thermo-hydraulic coupling. For this purpose, an integrated Monte Carlo burnup calculation code MCB is very suitable. However, statistical fluctuations, which are intrinsically present in Monte Carlo methods, need to be discriminate from an expected real solution. In case of HTR Monte Carlo modelling, flux oscillations and convergence problems with fission source may be brought about.

The MCB methodology in application for HTR core analysis is described in Chapter 2, while in the next Chapter 3 we present prepared high fidelity models of PUMA reactor used in our analysis. Chapter 4 contains analysis of physical conditions of an HTR in deep burn mode with plutonium and MA utilization, where influence of local conditions on nuclide time evolutions are assessed. The initial analysis of physical properties of HTR in deep burn is also presented there. Detailed core characteristics are described in Chapter 5, for both reference fuel options, with the chosen shuffling scheme adopted. We also investigated the CR operation concerning its influence on the local power deposition. Finally, the conclusions are presented in Chapter 6.

2. Monte Carlo burnup code system - MCB

The Monte Carlo Continuous Energy Burn-up Code (MCB) is a general-purpose code used to calculate a nuclide density evolution with time (after burn-up or decay). The code performs eigenvalue calculations of critical and sub-critical systems as well as neutron transport calculations in fixed source mode to obtain reaction rates and energy deposition that are necessary for evaluation of the burn-up. MCB internally integrates the well-known MCNP code (currently - version 5 [1]), which is used for neutron transport calculation, and a novel Transmutation Trajectory Analysis code (TTA) [2], which calculates density evolution, including on-line formation and analysis of transmutation chains. The code version MCB1C [3] became available to the scientific community on a freeware basis though Nuclear Energy Agency Data Bank, Package-ID: NEA-1643 since 2002. The MCB code has been developed recently and applied to neutronics and fuel cycle analysis of helium cooled reactor system in frame of EU FP5 project "PDS-XADS" [4]. Recent development of the code was directed towards advanced description of modern reactors, including double heterogeneity structures that exist in HTR-s. Current version allows users to define models that are more detailed, with larger number of universe levels, as well as to consider statistical fluctuation effects on Monte Carlo modelling of nuclear reactors. Below the methodology of core design and fuel cycle analysis using MCB is briefly described. The code is still under development; recently added features concern statistical analysis of burnup, emitted particle collection, thermal-hydraulic coupling, automatic power profile calculations, advanced procedure of burnup step normalization – so called "bridge scheme", and others.

2.1. General features of MCB

The main goal of a burnup code is to calculate the evolution of material densities. It concerns all possible nuclides that may emerge in the system after nuclides decays, transmutations, or particles emissions. Transmutation process includes fission product breakdown into nuclides as well as helium and hydrogen atoms formed from emitted α particles and protons respectively. There is no required predefined list of nuclides under consideration since all transmutation chains are being formed automatically on-line basing on physical conditions that constrain the system under the control of user-defined thresholds. These thresholds concern contribution to the nuclide mass change from constructed transmutation trajectories. In a real system under irradiation or decay, the nuclide composition undergoes evolution that generally can be described with a continuous function of time. An approximation of this function is obtained in MCB throughout time the step procedure which starts from assessing reaction and decay probabilities of every possible channel by means of stationary neutron transport calculations. In the next step, the transmutation chain is formed and then solved to produce nuclide density table in required time points. The main features of the code can be outlined as follows below.

- The decay schemes of all possible nuclides and their isomeric states are formed and analysed on the basis of the decay data taken from two sources. The first one – TOI.LIB, which is based on Table of Isotopes [5], describes decay schemes for over 2400 nuclides including formation of nuclides in the excited states.
- Numerous cross-section libraries and data sets can be loaded into computer memory to calculate adequately reaction rates and nuclide formation probabilities. It includes possibility of separate treatment of cross section for different burnable zones, to account for thermal effects, employment of energy dependent distribution of fission product formation, and energy dependent formation of isomer nuclides.
- Thermal-hydraulic coupling with POKE [6] is available for prismatic HTR.

- Reaction rates are calculated exclusively by continuous energy method with the usage of the point-wise transport cross-section libraries and, in case of lack of proper library, by using the dosimetry cross section library. The contributions to reaction rates are being scored at every instant of neutron collision occurring in cells filled with burnable material by using the track length estimator of neutron flux.
- Fission product yield is calculated from incident energy dependent distributions of fission products prepared separately for every fissionable nuclide.
- Heating is automatically calculated in a similar way as the reaction rates during neutron transport simulation by using heating cross sections, which are KERMA factors included in standard cross section tables. The code calculates automatically also the heating from natural decay of nuclides, what allows for consideration of afterheat effects. The energies of decays are taken from the ORIGEN library [7].
- Time evolutions of nuclide densities are calculated with the complete set of linear transmutation chains that is prepared for every zone and time step so it is being automatically adjusted to the transmutation conditions evolving with time.
- The code uses extended linear chain method, which is based on the Bateman approach, to solve prepared-on-line a set of linear chains that noticeably contribute to nuclide formation.
- Detailed analysis of transmutation transitions from nuclide to nuclide is performed. The transmutation chains that are formed by the code can be printed for nuclides of interest.
- Material processing is available along with material allocations to geometry cells during the burnup. Using this feature the user can simulate the fuel shuffling or CR operation.

2.2. Solution of Bateman equations

MCB adopts general solution of Bateman equations derived from linear chain method. The general transmutation chain, which is nonlinear, is resolved into series of linear chains using methodology of transmutation trajectory analysis. MCB is free from producing and using one-group neutron cross section. It uses transmutation probabilities instead, which are assessed directly in the process of neutron transport calculation executed independently for every transmutation zone and every time step.

Transmutation constants can be expressed as follows:

$$\lambda_{i,j} = b_{i,j}^{d} \cdot \lambda_{j}^{d} + \sum_{x=n,p,\pi} \int \Phi^{x}(E)\sigma_{i,j}^{x}(E)dE \qquad (1)$$

where the symbols denote:

λ_j^d - decay constant of *j*-th nuclide,

$b_{i,j}^d$ - branching ratio of *j*-th nuclide decay into *i*-th nuclide,

Φ^x - particle flux (*x* = neutrons, protons, pions +,0,-),

$\sigma_{i,j}^x$ -cross section for production of *i*-th nuclide by particles *x* during interaction with *j*-th nuclides.

The transmutation constants appear as the coefficients of the Bateman equations describing the general, non-linear transmutation chain for w nuclides as follows

$$\frac{\mathrm{d}N_i}{\mathrm{d}t} = \sum_{j=1,w} \lambda_{i,j} \cdot N_j \qquad (i = 1, w)\,. \tag{2}$$

2.2.1. Transmutation Trajectory Analysis

Usually, in the commonly applied numerical methods the set of linear chains is prepared arbitrarily, which is sufficient for well-defined cases. However, for a more general case the application of procedure that resolves the non-linear chain into a set of linear chains is necessary to assure the mass flow balance and the numerical solution stability.

In order to derive the solution of a general case basing on the known solution of a linear decay case, it is convenient to focus on the transmutation transition from one nuclide to the other one after elapsing time *t*. The transmutation transitions can lead through many paths, which possibly branch, forming a non-linear chain. Now, let us define a transmutation trajectory as a sequence of direct nuclide-to-nuclide transitions, starting from the first nuclide and ending at the last, *n*-th nuclide. The transmutation trajectory is almost equivalent to a decay chain, but due to an occurrence of branching in the non-linear chain, the mass flow is not preserved on a single trajectory level. It is preserved, however, over all the trajectories that can be extracted from the non-linear chain. The Bateman equations for transmutation trajectory representing a linear chain will have the following form:

$$\begin{aligned} \frac{\mathrm{d}N_1}{\mathrm{d}t} &= -\lambda_1\ N_1 \\ \frac{\mathrm{d}N_i}{\mathrm{d}t} &= b_i \lambda_{i-1} N_{i-1} - \lambda_i\ N_i \qquad (i = 2, n) \end{aligned} \tag{3}$$

where

$$\begin{aligned} \lambda_i &= \sum_{j \neq i}^{j=w} \lambda_{i,j} \\ b_i &= \frac{\lambda_{i,i+1}}{\lambda_i} \end{aligned} \qquad (i = 1, n) \tag{4}$$

The solution is following:

$$N_n(t) = \frac{N_1(0)}{\lambda_n} \sum_{i=1}^{n} \lambda_i \alpha_i \exp\left[-\lambda_i t\right] \tag{5}$$

where

$$\alpha_i = \prod_{\substack{j=1 \\ j \neq i}}^{n} \frac{\lambda_j}{(\lambda_j - \lambda_i)} \tag{6}$$

In a general case when certain transition can appear in the chain m_k times the solution takes more complicated form:

$$\mathrm{N}_\mathrm{n}(t) = \frac{\mathrm{N}_1(0)}{\lambda_\mathrm{n}} \sum_{i=1}^{n} \lambda_i \alpha_i \exp\left[-\lambda_i t\right] \cdot \sum_{m=0}^{\mu_i} \frac{(\lambda_i t)^m}{m!} \cdot \Omega_{i,\mu_i - m} \tag{7}$$

where

$$\alpha_i = \prod_{\substack{j=1,n \\ j\neq i}} \left(\frac{\lambda_j}{\lambda_j - \lambda_i} \right)^{m_j} \qquad \text{and} \quad \mu_k = m_k - 1 \tag{8}$$

The omegas for $i \in [1,n]$ and $j \in [0,\mu_i]$ take the following forms:

$$\Omega_{i,j} = \sum_{h_1=0}^{j} \sum_{h_2=0}^{j} \cdots \sum_{h_n=0}^{j} \prod_{\substack{k=1 \\ k\neq i}}^{n} \binom{h_k + \mu_k}{\mu_k} \left(\frac{\lambda_i}{\lambda_i - \lambda_k} \right)^{h_k} \delta\left(j, \sum_{\substack{l=0 \\ l\neq i}}^{n} h_l \right) \tag{9}$$

The concentration of the last trajectory nuclide due to the trajectory transition can be written as:

$$N_n(t) = N_n(0) \frac{B}{\lambda_n} A(t) \tag{10}$$

where

$$B = \prod_{k=1,n-1} b_k \tag{11}$$

is the total trajectory branching rate. The disintegration or removal rate of the last trajectory nuclide can be expressed as follows:

$$A_n(t) = N_n(0) \cdot B \cdot A(t) \tag{12}$$

It can be thought of as generalized activity. The time integral of the removal rate (19) leads to the following function:

$$I(t) = \int_0^t A_n(t)dt = N_1(0) B \sum_{m=0}^{\mu_i} \Omega_{i,\mu_i - m} \cdot f_{i,m}(t) \tag{13}$$

where

$$f_{i,m}(t) = 1 - \exp\left[-\lambda_i t\right] \cdot \sum_{k=0}^{m} \frac{(\lambda_i t)^k}{k!} \tag{14}$$

The above stands for the sum of the nuclides concentrations of formed in the disintegration process of the *n*-th nuclide or their daughters after being produced from the transition along considered trajectory. For given time *t*, every transmutation trajectory can be characterized by two quantities: the trajectory transition

$$T(t) = N_n(t) / N_1(0) \tag{15}$$

and the trajectory passage

$$P(t) = I(t) / N_1(0) \tag{16}$$

The transition and passage functions are important for the mass balance of transmutations, which is an ultimate parameter for checking correctness and convergence of any numerical algorithm for calculation of time evolutions of concentrations in a transmutation system. They are used to control the numerical algorithm of breaking down a non-linear transmutation chain into a series of transmutation trajectories for which the concentration can be calculated.

2.2.2. Fission product transmutation modelling

The equations derived can be also adapted for the case of continuously supplied nuclides such as nuclides yielding form the fission product. In this case, the concentration of nuclide that starts a transmutation trajectory is described as follows

$$\frac{\mathrm{d}N_1}{\mathrm{d}t} = -\lambda_1 N_1 + s_1 \tag{17}$$

where s_1 is the nuclide production rate. The production rate, s_1, can be represented by the decay of an artificial nuclide N_0 that is characterized by decay constant λ_0 and branching ratio b_0, which need to be set to satisfy the following conditions:

$$N_0(0) = s_1 t \quad \text{and} \quad N_i(0) = 0 \quad \text{when} \quad i > 0$$

and (18)

$$\lambda_0 = \frac{1}{t} \cdot \ln \frac{b_0}{b_0 - 1} \text{ where } b_0 >> 1$$

As b_0 is set arbitrarily as a large number, the λ_0 constant results from equation (18) for a given value of the required production rate s_1. The case of continuously supplied nuclides takes places when fission products are produced with assumed constant rate of the actinides fissioning.

2.3. MCB added values in applications for HTR analysis

Due to existing complexity of burnup process and reactor physics itself in an HTR, in order to ensure high quality of design, particularly with its safety features, it is reasonable to apply few different tools of reactor core analysis. This can bring about results obtained from few different perspectives. Here, the Monte Carlo methods, although demanding more computer power, are characterised by higher level of model complexity and fidelity, thus the results can be obtained in an integrated way, possibly displaying important effect that can be hidden or neglected in another approach. For this purpose, an integrated Monte Carlo burnup calculation code MCB is very suitable. It is fully integrated calculation system, which allows the user taking into consideration of spatial effects of full heterogeneous reactor model with continuous energy representation of cross section and the thermo-hydraulic coupling. Here, a particular importance lays in a proper assessment of the power distribution, but not merely at BOL but as a function of burnup with consideration of the CR operation. The power distribution affect many core safety features, therefore a simplified approach can lead to biased conclusions. As Monte Carlo approach presents some benefits, it is not free from their intrinsic problems, which need to be treated accurately. Namely, statistical fluctuations, which are intrinsically present in Monte Carlo methods, need to be discriminate from an expected real solution. In case of HTR Monte Carlo

modelling, flux oscillations and convergence problems with fission source may be brought about.

2.3.1. Thermal-hydraulic coupling with POKE

Introduction of thermal hydraulic calculations into Monte Carlo simulations was done by coupling MCB with the POKE code [6]. The POKE code was written in GA; its original version was designed for the geometry and parameters of Ft. St. Vrain reactor, and later it was used for GT-MHR analysis as well. POKE determines fuel and coolant temperature distributions as well as coolant mass flow in the steady state. The reactor configuration consists of a number of parallel coolant channels connected to common inlet and outlet plenums. The reactor between the inlet and outlet plenums is divided into inlet reflector, core and outlet reflector. All heat is assumed to be generated in the core. For calculational purposes the reactor is divided into a number of cylindrical regions, which extend from the inlet to the outlet plenum. The POKE code iteratively solves three one-dimensional equations that express the conservation of mass, momentum and energy for each channel modelled. The coolant mass flow rate results from balancing the pressure drop from the inlet to the outlet plenum.

The code coupling was done on the level of source code, where the modified version of POKE has been incorporated into the MCB code, but all the data exchange between codes has been left on external files, in order to allow the user to recalculate. The thermal-hydraulic specification is read in from the POKE input file, which describes the reactor geometry and other parameters, whereas MCB delivers only the power distribution profile. The temperature profile at BOL is to be defined by the user after arbitrary assumptions or using the results obtained in earlier calculations. Invoked POKE calculates the required thermal hydraulic parameters as well as the new temperature profiles. On that basis the new temperatures of all regions together with the cross sections adjusted to the temperature are used for new power profile iteration, and the subsequent burnup calculations provides more realistic isotope production results.

2.3.2. Bridge scheme of burnup step

Statistical fluctuation in Monte Carlo modelling should in general follow the law of large numbers of the probability theory. On this assumption, the standard formulations of statistical measures of probability distribution are used in Monte Carlo neutron transport calculations. However, in some nuclear reactor systems like HTR, the fluctuation of the calculated power distribution contains a systematic term, which is propagated in consecutive neutron generations through the fission source distribution. In burnup calculations scheme the process of source normalization to the constrained power is done usually using the neutron heating rate as evaluated at the beginning of step. In this treatment, the systematic term (in the fluctuation of power distribution) tends to conserve itself or to form increasing oscillations. This process of creating oscillations is linked with production and depletion of Xe135 in a deeply moderated HTR core. Here we do not mean the real physical oscillations, which can be created also, but the numerical oscillations in the calculated density distribution. Another source of systematic term is related directly to the neutron source convergence problem, which occurs when the fundamental distribution of the source is difficult to achieve, even if the reactivity converges early. This behaviour occurs in large HTR cores, which was studied in more details in KTH work [8].

The magnitude of both effects can be reduced when the source normalization procedure is improved. This is done in so-called bridge scheme of burnup step, in which the normalization is done using the step average functions. This procedure involves repeated calculation of the neutron heating rates and reaction rates at both step ends – beginning of step (BOS) and end of step (EOS) as shown in Figure 1. In the

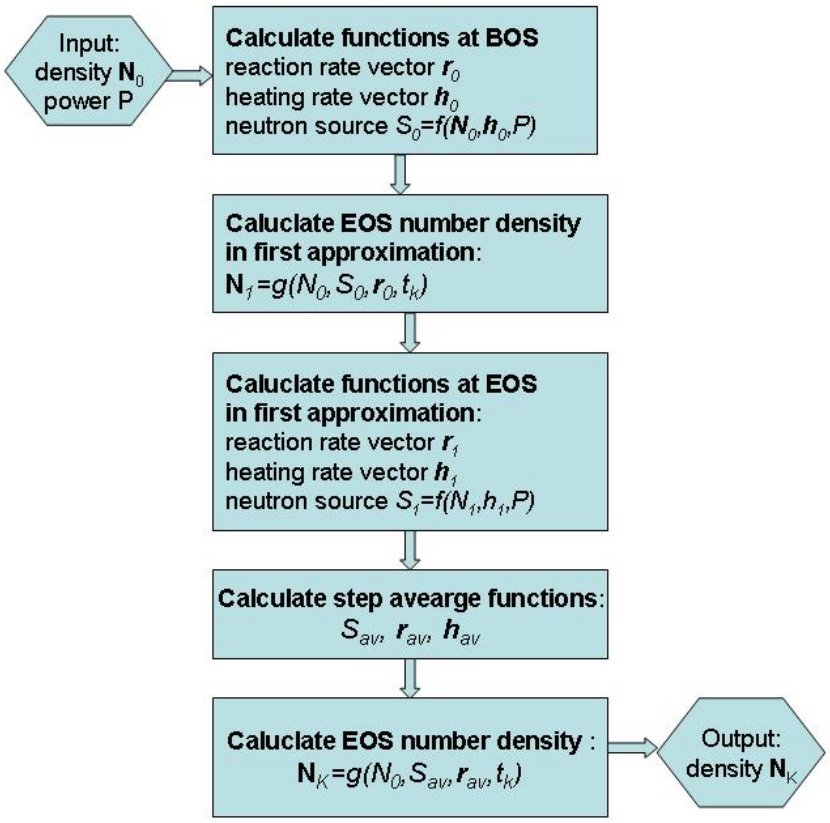

Figure 1. Diagram of bridge scheme of burnup step

first approximation the number density at EOS is calculated with assumption of constant heating and reaction rates over the entire step. This may result in biasing of the burnup if reaction or heating rates change with time. A correct calculation of final number density requires the average values of the neutron source strength and reaction rates. The process of averaging uses a simple average of two values: at BOS and at EOS after correction. The EOS correction in done in a step predictor module, in which the reaction rates and source strength of the first approximation are scaled by the ratio of the burnup constrained to its first approximation.

3. HTR reactor calculation model

The PUMA prismatic core model for MCNP/MCB calculations was prepared according to the reference specification from Deliverable 121 (D121) [9], with recommended design option concerning axial-only fuel shuffling and 4-batch refuelling scheme. The major objective of our Monte Carlo study is to understand deeply the neutronic and burnup characteristic of the deep burn core in the reference configuration by consideration of that core features in the models that were neglected so far, or are difficult to be considered using other methods. We pay a particular attention to the modelling of CR operation as the CR insertion level is adjusted along with the reactivity loss during burnup. The reference PUMA reactor core comprises five radial rows of fuel blocks in eight axial block layers. For the power distribution analysis and burnup calculations, the active core is divided into burnup zones. Every fuel block row is divided radially into two halves, while axially every block layer is divided into three regions, which altogether constitute 240 fuel zones. The core was

filled with fuel compacts containing TRISO in 18% volume fraction. The exact locations of the radial regions used in thermal hydraulic calculations and fuel burnup are shown also in Figure 2. The active core is model with high level of fidelity with

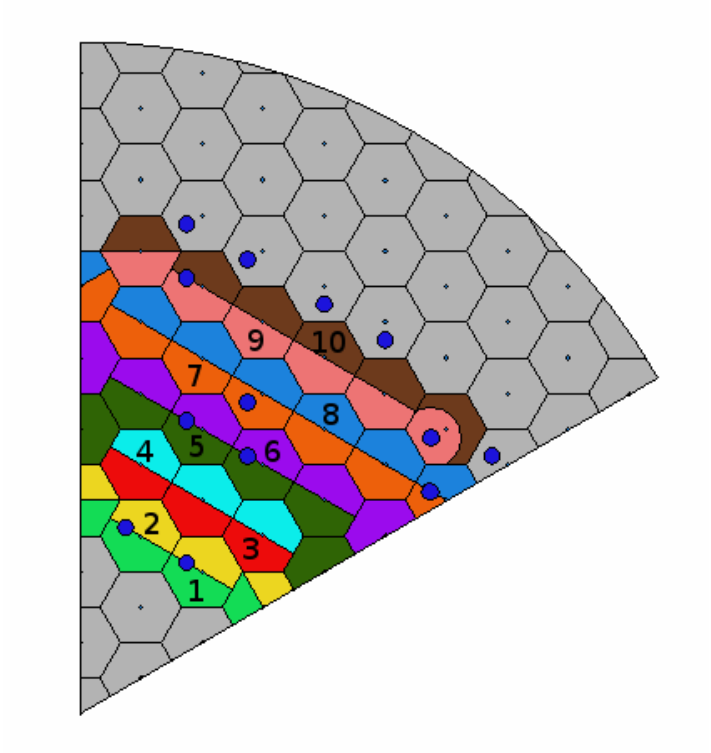

Figure 2. Radial division of active core

full description of details including the fuel double heterogeneity. The fragment of the core model is shown in Figure 3, where different colours denote different zones with their materials and corresponding temperatures. It can be observed that the core structure is already very complicated, but in fact each fuel rods has its own internal structure shown in Figure 4, where the fragment of hexagonal spheres) can be seen. In the applied model, apart from the fuel, also burnable poison rods constitute burnable zones in number of 80; 10 radial regions times 8 axial zones. The CR channels are also axially divided in order to allow for modelling of CR operation, which follows the reactivity loss with burnup. Concerning the fuel shuffling, we have applied recommended axial- only shuffling scheme with the mirror symmetry in respect to the core middle plane, as is shown in Figure 5. This is one of the simplest schemes, which reduces the space of an operator error and shortens the outage time required for shuffling, as compared with radial or mixed axial-with-radial shuffling schemes.

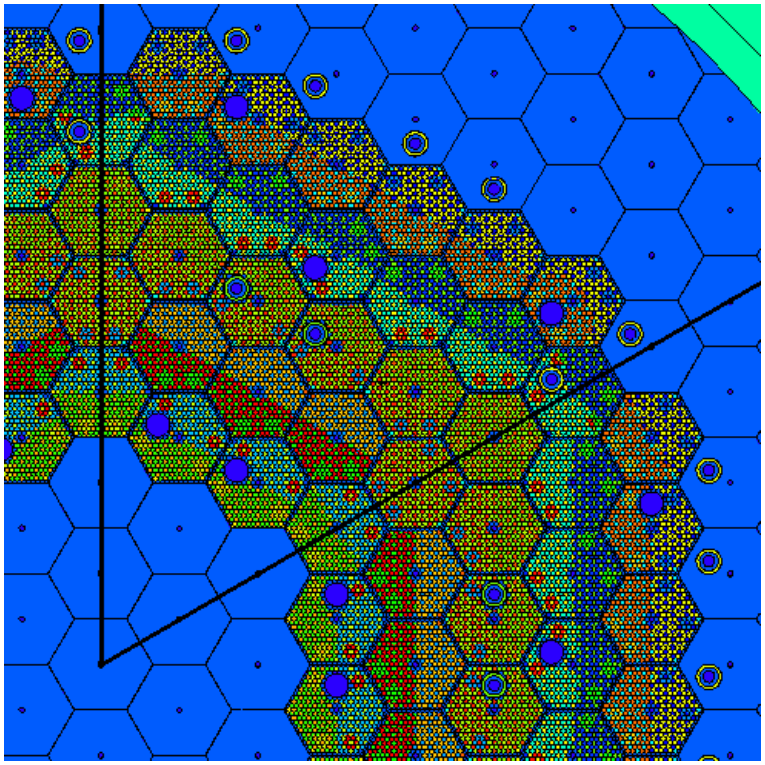

Figure 3. Core regions with fuel rods and CR/RS holes

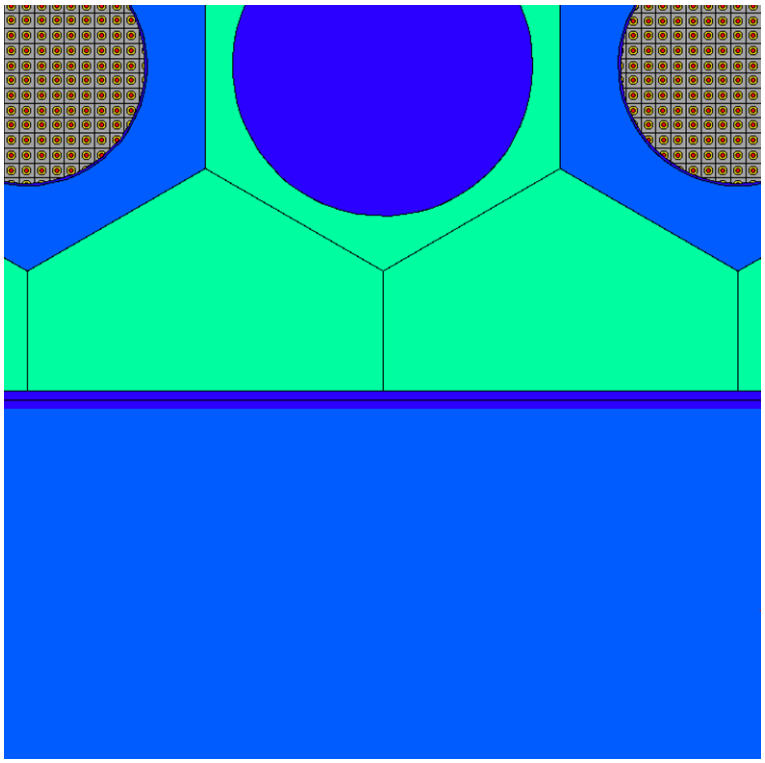

Figure 4. Details of the fuel block structure

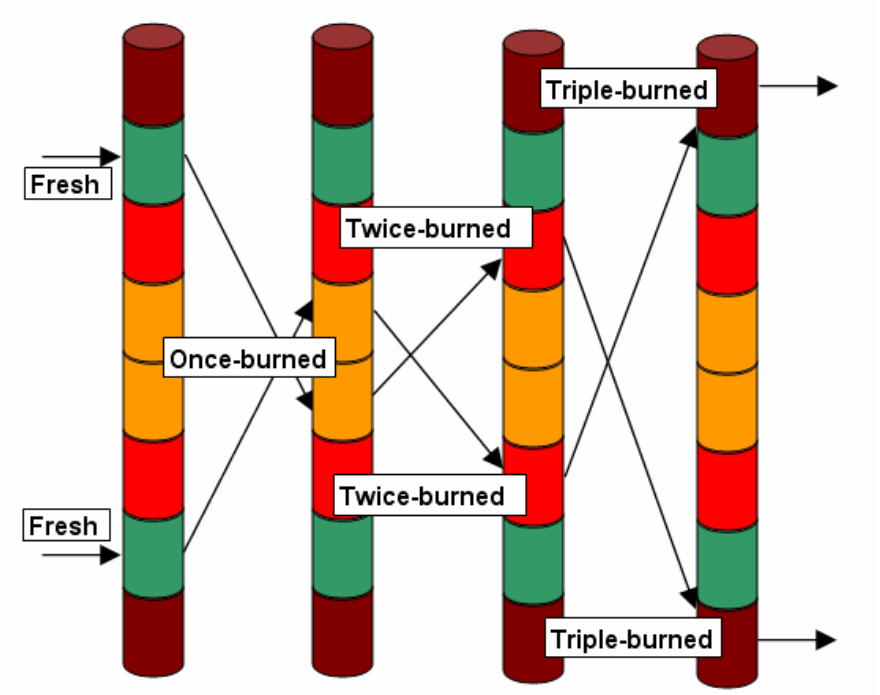

Figure 5. Scheme of 4-batch axial-only block shuffling

The adopted core design features are summarised below.

- The eight fuel-block layers design has been applied.
- The four-batch axial only shuffling scheme has been chosen.
- The core has been divided into burnup zones in 10 radial regions and 24 axial segments, which makes 240 fuel burnable zones.
- Control rods operation has been modelled with insertion level adjustment of 50 cm bins.
- Reserve shutdown channels have been modelled and filled by helium.
- Burnable poisons rods have been applied only in the inner region (inner half of the 4-th block row). Eu_2O_3 rods with density of 7.4 g/cm^3 have been used. Remaining burnable poison holes have been filled with helium.
- All coolant holes have been modelled in the blocks of active core and axial reflectors.
- Reduced height of the channels located under dowels has been modelled.
- The fuel handling holes have been modelled.
- The second reference fuel composition with MA content, as shown in Table 1 is our primary choice, while the first vector is an option used in comparative analysis.
- In the course of the study, the cycle lengths have been adjusted, according to the manageable reactivity margin, to 420 days for the “first reference fuel composition” and to 350 days for the “second reference fuel composition”.

Table 1. Reference fuel compositions [9].

	Fraction, wt%	
Nuclide	First vector	Second vector
Np-237	-	6.8
Pu-238	2.59	2.9
Pu-239	53.85	49.5
Pu-240	23.66	23.0
Pu-241	13.13	8.8
Pu-242	6.78	4.9
Am-241	-	2.8
Am-242m	-	0.02
Am-243	-	1.4

4. Reactor physics calculations for deep burn of Pu/MA

Since the PUMA core in deep burn design has to achieve as high burnup as possible, we need to understand which physical processes play the major role in transmutation and burnup. We also need to know what the dependences on the local conditions occurring in the core are. This knowledge is vital in order to make proper design decisions that will bring about an effective and safe design. Concerning the safety aspects, not only reactivity control is important, but also an acceptable power distribution. This concerns not only power generated during operations but also the afterheat distribution, which should be manageable during possible LOCA accidents. Although the analysis of LOCA accident is beyond the scope of this project, a neutronic analysis can identify safety threats possibly implied in incorrect designs. In this chapter, we present reactor physics analysis of deep burn design comprising of transmutation analysis, power distributions during operation and the impact of reactivity control on power and temperature distributions.

4.1. Transmutation analysis

In a deep burn design, the process of transmutations is a primary driver of power distribution in that the heavy metal nuclides can fission out early or contribute to the transmutation chains that are leading to either non-fissile or fissionable nuclides. In the first case this can increase afterheat globally or locally in the long term, whereas in the second - contrary case, reduce the reactivity loss. Since the neutronic conditions in HTRs differ strongly depending on the location within the core due to the local temperature and the reflector distance, we have analysed what is the characteristics of transmutation process in the PUMA core. The transmutation chain distribution depends on the reaction branching, which is presented in
Table 2. This analysis has been performed in the static burnup conditions of the PUMA core entirely filled with the fresh fuel. This model would reflect reality only in the real case single-batch refuelling scheme where the power peaks in the vicinity of inner reflector as a result of unacceptable power distribution.

Table 2. Reaction branching dependence on location; second ref. fuel case

Location:	**Description**	**Inner column (4^{th} block row's inner half)**			**Middle row column (6^{th} block row's outer half)**		
	Radial region	1	1	1	6	6	6
	Axial segment	1	15	24	1	15	24
Conditions	Flux 10^{14} n/cm^{2}s	1.75	2.25	1.27	1.2	1.33	8.03
	50 day step burnup MWd/kg HM	72.97	84.77	55.04	32.63	28.62	23.20
Neutron capture branching	Pu238 → Pu239	88.42%	86.90%	85.01%	79.89%	75.63%	74.70%
	Pu239 → Pu240	37.04%	37.60%	37.51%	37.58%	38.45%	37.76%
	Pu240 → Pu241	99.51%	99.57%	99.53%	99.47%	99.57%	99.48%
	Pu241 → Pu242	23.66%	23.95%	23.49%	21.74%	20.95%	20.52%
	Pu244 → Pu245	99.92%	99.94%	99.92%	99.94%	99.96%	99.94%
	Am241 (n.γ)	98.89%	98.91%	98.80%	98.58%	98.62%	98.36%
	Am241 → Am242	78.40%	78.60%	78.30%	78.12%	78.60%	78.03%
	Am241 → Am242m	20.49%	20.31%	20.50%	20.46%	20.02%	20.33%
	Am242m → Am243	18.54%	18.26%	18.43%	17.80%	17.25%	18.20%
	Am243 → Am244	99.59%	99.63%	99.58%	99.60%	99.68%	99.58%
Decay branching	Pu238 → (α) U234	4.54%	4.58%	7.14%	10.31%	12.05%	15.29%
	Am241 → (α) Np237	0.22%	0.19%	0.31%	0.45%	0.44%	0.69%
	Pu241 → (β) Am241	5.31%	5.14%	7.72%	12.35%	14.45%	17.71%
Fission branching	Pu238 → FP	7.04%	8.52%	7.85%	9.79%	12.32%	10.00%
	Pu239 → FP	62.96%	62.40%	62.49%	62.41%	61.54%	62.23%
	Pu241 → FP	71.04%	70.91%	68.79%	65.90%	64.60%	61.77%
	Am241 → FP	0.89%	0.90%	0.89%	0.97%	0.94%	0.95%
	Am242m → FP	81.46%	81.74%	81.57%	81.88%	82.75%	81.80%
Ratio: (n.γ)/fission	Pu238	12.56	10.20	10.84	8.16	6.14	7.47
	Pu239	0.588	0.603	0.600	0.602	0.625	0.607
	Pu241	0.075	0.072	0.112	0.187	0.224	0.287
	Am241	112	110	111	102	105	103
	Am242m	0.228	0.223	0.226	0.217	0.208	0.222

What is important here, the burnup rate varies depending on local position by factor of four, which can have an adverse effect on the power distribution. Leaving aside the

question whether this power distribution can be levelled out by burnable poison, let us focus on transmutation analysis. As fission reaction contributes the most significantly to the burnup, the fission rate serves here as a point of reference. The product of reaction branching and destruction rate is a good measure of the respective reaction rate. Reaction branching to fission is responsible for the ultimate heavy metal nuclide destruction, which terminates the possibility of further transmutation. If a heavy metal nuclide avoids fission it can become an active actinide contributing to afterheat, mostly in alpha decay. The fissionable nuclides under considerations are Pu239, Pu241, Am242m, Cm243 and Cm245. All plutonium isotopes have substantial probabilities of fission avoidance, higher than 1/3; therefore significant fraction of them can be transmuted into non-fissile ones. We observe significant dependence on location of the branching in case of three nuclides: Pu238, Pu241 and Am241. The formation of Am241 from Pu241 strongly depends on the location, mostly due to different burnup rates. Similar case occurs with direct alpha decay, which contributes stronger in locations with lower burnup rate. Ratios of neuron capture to fission shown in the bottom of
Table 2 indicate an increase of neutron capture with lower burnup in case of Pu238 but a decrease in the case of Pu241. The effect of cross section dependence on fuel temperatures plays here some role. The lower temperature in the upper locations enhances neutron capture of Pu238 while suppresses its fission. Other effects also occur but on lower amplitude. Nevertheless, they lead to different nuclide evolution patterns depending on the locations. General conclusions of this study are as follows.

- Local conditions in uniform core are causing non-uniform burnup distribution.
- Non-uniform burnup distribution results mostly form variation of fission to capture ratio depending on locations.
- In the locations with low burnup rate, increased fissile destruction by neutron capture occurs, which leads to a steeper reactivity swing, thus lowering achievable burnup on discharge.
- The axial buckling of the neutron flux needs a correction, particularly in the inner column, which might be obtained with introduction of axial shuffling.

4.2. Power distribution in equilibrium cycle in 4-batch shuffling scheme

Power distribution in an HTR with prismatic core uniformly loaded with fuel is characterised by power peaks near reflectors that might lead to unacceptable temperature level. This is presented in Figure 6 where the temperature peaks at the level of 1300 ^{o}C, exceeding its acceptable limit. It should be noted that within the hottest fuel block the temperature could differ by about 300 degrees. This observation necessitates the usage of a model with radial segments thinner than a block row; otherwise, the results of temperature calculation will be biased and too optimistic. Distributed burnable poison introduction to the core can effectively lower power peaks. One can expect similar influence on the core power distribution from the fuel axial shuffling. For the assessment of power distribution, we have performed calculations in the full core burnup model with four-batch axial-only block shuffling, according to the recommendation from D121. Applied scheme of fuel shuffling is presented in Figure 5. Burnable poison rods have been applied only in the first radial region, i.e. the inner half of the first fuel block row. We have applied both reference fuel vectors in order to reach the equilibrium cycle. The current Monte Carlo analysis has shown that with the first reference fuel, which is without minor actinide content, it is possible to achieve an equilibrium cycle of 420 days in four reloading batches, which sums up to 1680 full power days of irradiation. For the second case of fuel, with minor actinides content, the cycle length is shorter due to the lower amount of fissionable nuclides and equals 350 days summing up to 1400 full power days.

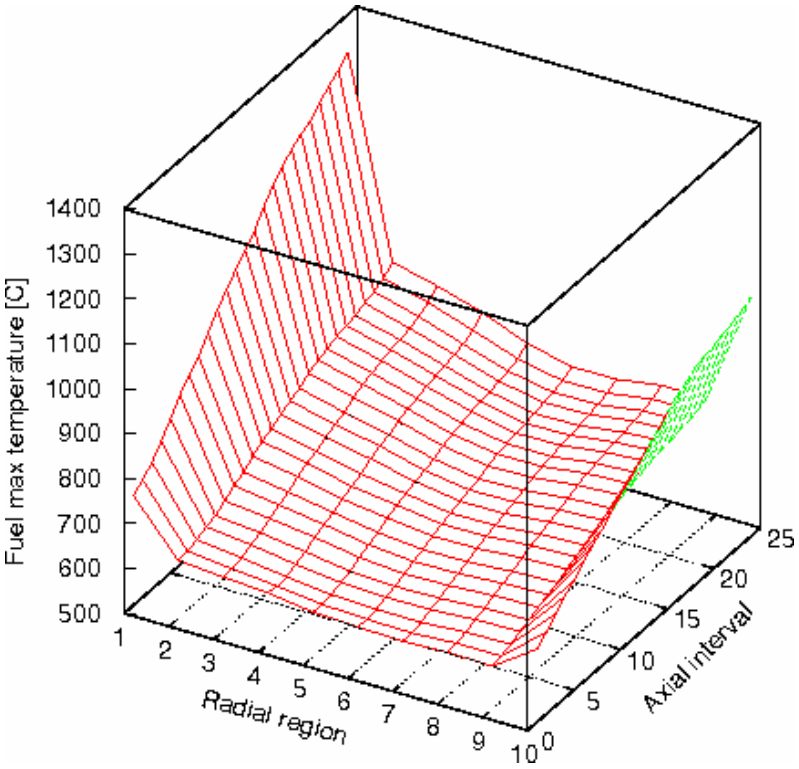

Figure 6. Fuel temperature distribution in uniformly loaded PUMA core.

4.2.1. Reduction of power spatial oscillations

Applied burnup calculation model includes the bridge scheme of burnup in order to account for numerical oscillation of the neutron flux, as well as to adjust the power normalization to the heating rates, calculated as step average values instead of BOS values. The flux oscillations that occur in the thermalized neutron spectra originate from two sources: Xe135 unsteadiness and fission source convergence. The real concentration of Xe135 can have spatial oscillations caused by a local tilt in neutron flux, which changes the balance between its production and destruction rates. A global reduction or increase in neutron flux can also lead to the global oscillations of Xe135, which in return directly affects the neutron flux. A phenomenon of similar nature occurs in Monte Carlo calculations of the neutron flux in such a system. Here, calculated local flux oscillations at BOS change their distribution at EOS due to a feedback effect; flux oscillation vector changes its phase angle by 180°. This effect is presented in Figure 7. The occurring power oscillations have a collective nature; areas of power oscillations in the same direction exceed the fuel block dimensions. Since the average values have been used for the burnup step, these power oscillations have been reduced in our results of power distribution.

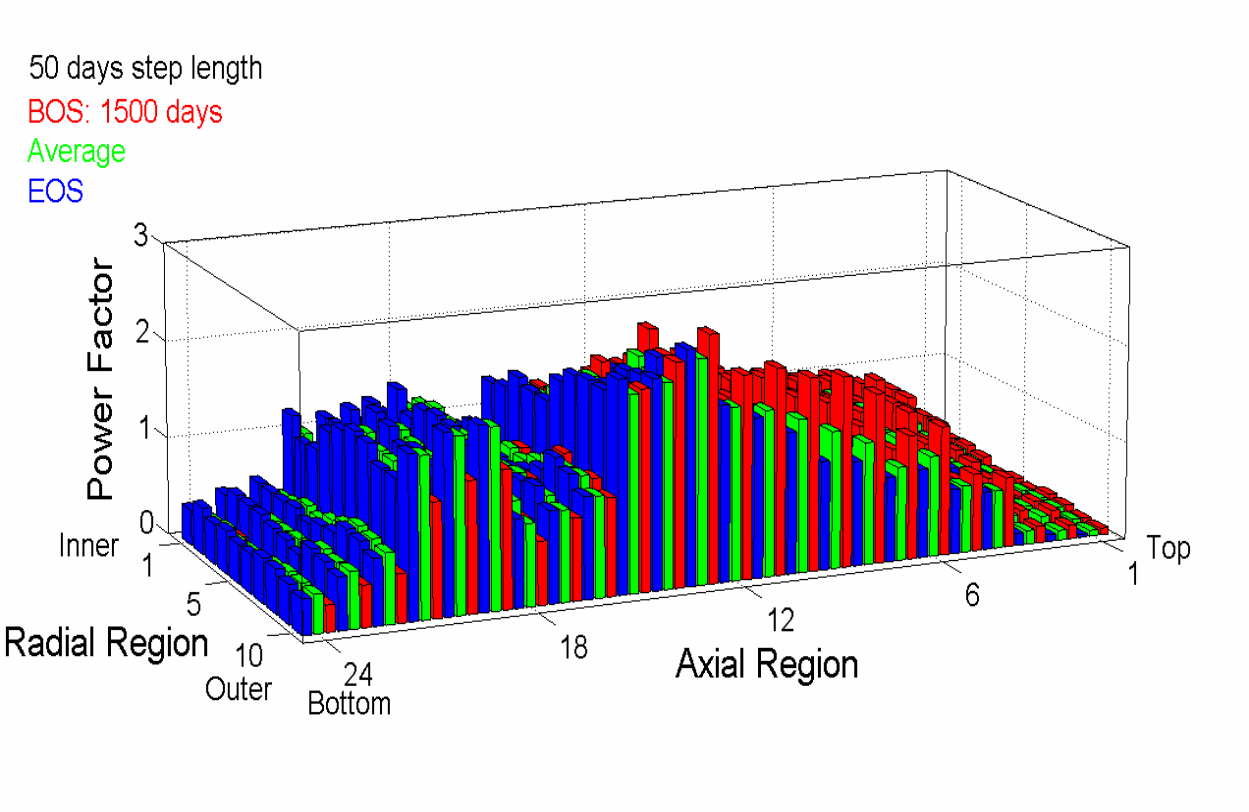

Figure 7. Power spatial distributions in the bridge scheme of burnup step

4.2.2. Influence of CR operation on power distribution

Modelling of CR operations is not often being included in core performance assessments, due to complexity it involves. However, locations of power peaks and assessments of power and temperature peak values can be strongly affected by the CR operations, particularly in PUMA - like systems, due to the short neutron transport length. Moreover, the influence of CR operation on the power distribution might be stronger in fuel batch reloading schemes. Therefore, before any optimization of fuel refuelling and shuffling can be undertaken, the assessment of CR operation needs to be accomplished. As the axial only shuffling scheme has positive influence on the power distribution by leading to reduction on power peaking near reflectors, we need to asses how the CR operation influences it. This analysis has been carried out, where CR operation were modelled by changing the CR insertion level stepwise linearly in 100 cm bins along with the fuel burnup. The time evolution of power profile is depicted in Figure 8, which concerns equilibrium cycle of 350 days with the second reference fuel. The graphs apart from the first one on the figure show the step average distributions, where the basic step duration of 50 days has been used. At the cycle beginning, two shorter steps were applied in order to stabilise Xe135. The power ratings for three characteristic points: after 5, 150 and 350 days are presented in the Annex appended to this report. At BOC the operational CR were fully inserted while the start-up CR were fully withdrawn. The power distribution then was quite well balanced; the BPR suppressed power peaking close to the inner reflector while in the central location of axial direction the power peak is reduced due to the fuel partially burned. The power generated in the upper core half is grater than in the lower. This results from lower temperature in the upper part, which negatively changes the reactivity. The power ratings in radial outer regions are generally lower than the average, due to CR influence, which reduced the reflector significance. In the next steps the CR have been gradually shifted, which brings about a significant change in the axial power profile.

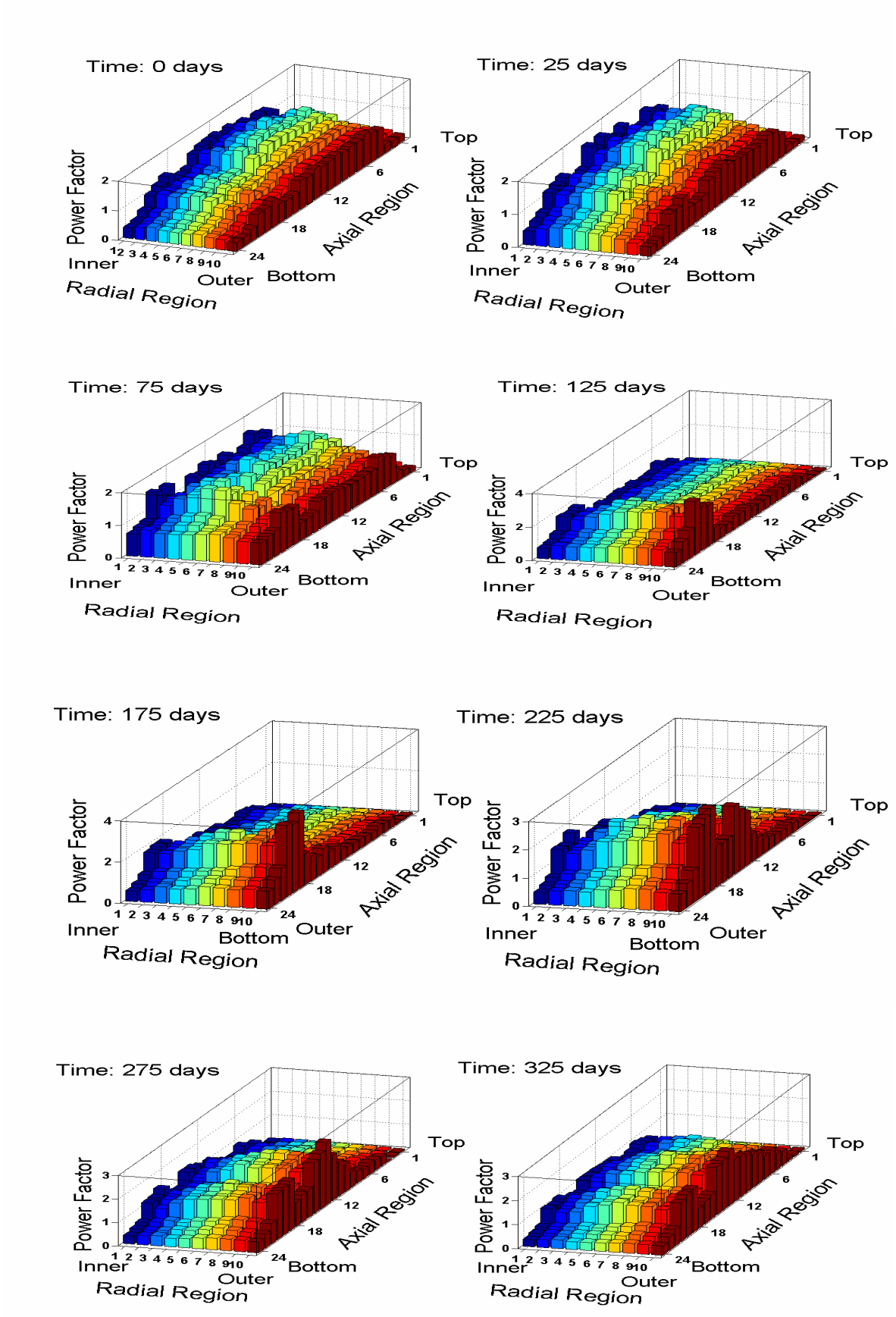

Figure 8. Power profile in cycle with CR operation modelled; Pu+MA fuel, 350- day 4-batch equilibrium cycle in axial only shuffling.

When the insertion level of CR became smaller than 600 cm, the 7-th block layer, with the fresh fuel became uncovered by CR, thus allowing the power to grow there, which should be expected generally. The second quarter of the cycle presents the highest power factors, exceeding four, which is more than twice bigger than at BOC. During that time, the most of the power was generated in the lower half of the core. The range of changes in parameters related to the power distribution is significant, which is shown in Table 3. The power profiles reach their maximum after about 150 days due axial profile change; the radial profile gets lower with burnup slightly.

Table 3. Core parameters related to the power at three characteristic time points of 350-day cycle.

Parameter	5 Days	150 Days	350 Days
Fuel kernel average power density [kW/cm^3]	3.56		
Fuel kernel maximum power density [kW/cm^3]	7.33	16.87	12.90
Maximum axial form factor	1.768	4.056	3.113
Average radial form factor	1.264	1.169	1.162
Total form factor	2.056	4.739	3.618

It is worth noting that the power peaks at the outer radius, whereas the radial profile is not a matter of concern as is shown in Figure 9 and there is no need for an additional power profile tailoring with burnable poison in regard to the radial power distribution. The observed increased power generation in outer regions during the second half of the cycle is caused primarily by its suppression early in the cycle. The CR operation increases the contribution to the total power from the lower half of the core. This is reflected in the distribution of the discharge burnup, which is presented in Table 4 and Figure 10. Since the burnup is not linear in time and its highest rate occurs during the first cycle, the fuel loaded into the lower layer undergoes a deeper burnup. The shuffling cannot compensate the difference in achieved burnup, which spreads up to 12% concerning the fuel loaded in upper and lower layers. Radially the burnup spread is about 22 %. Probably, there is room for improvements concerning burnup distribution by optimization of burnable poison distribution, or implementation of an asymmetric shuffling scheme. The obtained results concerning axial profile bring in a safety concern in relation to afterheat. During a certain period in the middle of cycle, the power is concentrated in 7th block layer and potentially high afterheat in case of a LOCA will need to be diffused. This problem needs to be investigated since it can be the source of a possible serious safety threat.

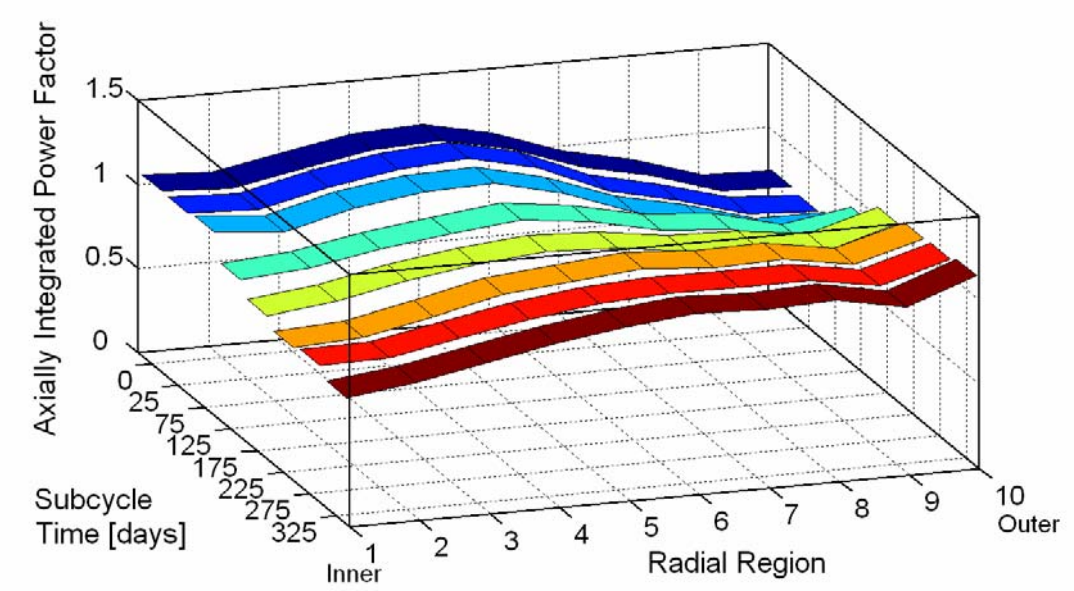

Figure 9. Axially integrated power profile with CR operation modelled; Pu+MA fuel, 350-day 4-batch equilibrium cycle in axial only shuffling.

4.2.3. Distribution of discharge burnup

Table 4. Distribution of discharge burnup in 4-batch 350-day cycle with 2nd reference fuel.

Location	Radial region										
	1	2	3	4	5	6	7	8	9	10	***Average***
Burnup MWd/HMt											
2nd layer load	448.2	455.8	493.0	527.4	547.7	531.5	489.4	467.4	425.0	458.3	***485.2***
7th layer load	465.2	473.6	521.1	557.0	575.6	567.8	534.1	527.5	481.2	524.7	***527.4***
Ratio of local to average								**Total average →**			**506.3**
2nd layer load	0.89	0.90	0.97	1.04	1.08	1.05	0.97	0.92	0.84	0.91	
7th layer load	0.92	0.94	1.03	1.10	1.14	1.12	1.05	1.04	0.95	1.04	

The results presented above show that the CR operation reverses the axial power distribution, as compared to the results obtained in models without CR operation modelling. Therefore, neglecting of this modelling will result in biased distributions and should be avoided. In reality, the temperature distribution effect on the power distribution is overshadowed by a counter effect resulting from the CR operation.

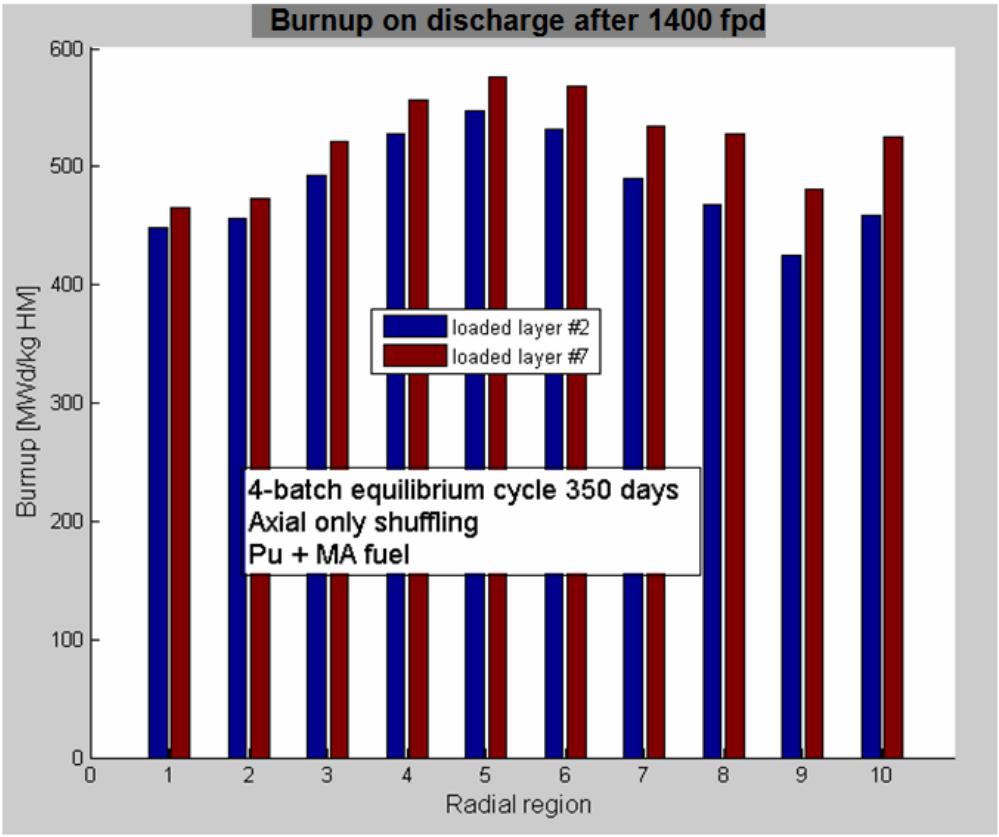

Figure 10. Distribution of burnup on discharge with effect of CR operation

4.2.4. Thermal-hydraulic assessment

The thermal hydraulic calculations for the analysed cycle were performed using POKE, which was invoked at the beginning of every step, with the power distribution assessed with MCB. The results obtained in the three characteristic points of the cycle are shown in Table 5 below.

Table 5. Thermal-hydraulic parameters in 4-batch 350-day cycle; 2nd reference fuel.

	5 day	150 day	350 day	Limit	
Power (total core)		600.0			MWth
Coolant inlet temperature		491.0			°C
Average coolant outlet temperature		851.6		851.6	°C
Maximum coolant outlet temperature	919.4	934.2	931.2	1021.0	°C
Coolant flow rate (total core)		320.0		320.0	kg/s
Bypass flow fraction		0.2			
Maximum fuel temperature	1023.4	1187.5	1076.4	1218.0	°C
Average fuel temperature	893.6	735.9	759.1	891.0	°C
Maximum graphite temperature	973.8	1055.3	1022.4	1142.0	°C
Average graphite temperature	766.6	706.8	729.9	770.0	°C
Core inlet pressure		7.067		7.100	MPa
Core pressure drop	0.040	0.037	0.038	0.050	MPa

Two first points are more representative than BOC and MOC respectively, since after 5 days the Xe135 mass is stabilised while 150-day point is the point of maximum of temperature. Detailed temperature distributions at these points are presented in the Annex appended to this report. The thermal-hydraulic parameters are under constraints during all the cycle. The fuel temperature at its maximum occurs at the middle point, due to the effect of CR withdrawal above the 7th layer, where the fresh fuel was laded.

4.3. Reactivity control in equilibrium cycle in 4-batch shuffling scheme

The length of equilibrium cycle in our reference case (G1) been evaluated as 350 full power days, where the main limiting factor was the criticality level at EOC. The reactivity change during the cycle is manageable by set of operational CR even with a margin of 980 [pcm] as is shown in Table 6 along with other reactivity changes and the control margins. The cycle length is shorter than desirable 420 days, which was possible to obtain with 1st reference fuel. There is a room for increasing the cycle length by a better burnable poison implementation, which can reduce the level of

Table 6. Reactivity change versus control margin; 2nd reference fuel

Reactivity change / reactivity margin	[pcm]
CZP to HZP	-2020
HZP to HFP – Xe135 buildup on power	-2430
CZP to HFP – startup reactivity change	-4450
Startup CR worth	8400
Cycle reactivity loss (350 fpd)	-4580
Margin for Xe135 buildup after shutdown	-1000
Required operational reactivity	-5580
Operational CR worth	6550

criticality, probably. As it is shown in Figure 11, the applied amount of burnable poison, which primarily has been adopted in order to reduce the power peaking in fresh fuel, actively consumes neutrons for all four cycles. Applied burnable poison in form of rods probably can be improved in order to reduce its inventory.

The fuel cycle in our studies has been analysed with simulation of CR operation, which is presented in Figure 12. In the applied scheme, the CR operation has been simulated in equal shifts, which does not represent the reality, and requires a better adjustment to the actual reactivity swing rate. In the simulation, the start-up CR-s haven't took part, therefore the initial drop of reactivity due to Xe135 build-up occurs. Later, the simulated CR movement is too slow, and then too fast, which is the effect of the fresh fuel uncovering by CR-s and Xe135 balance.

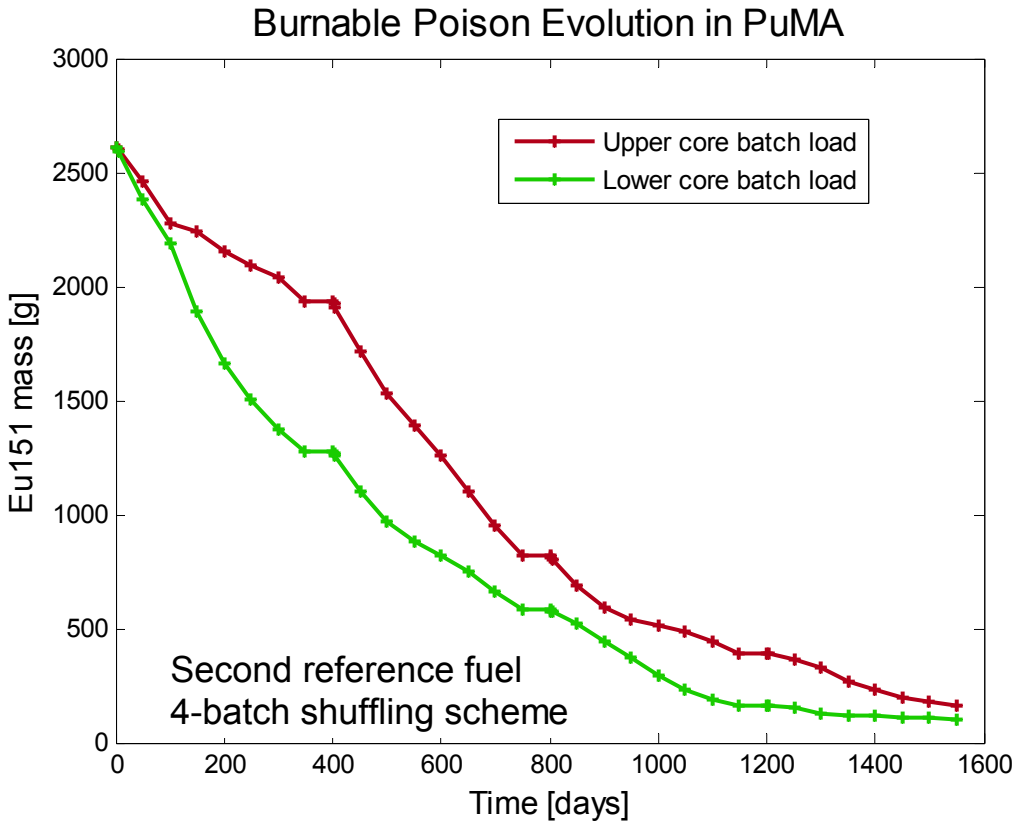

Figure 11. Burnable poison mass (Eu151) evolution in 4-batch shuffling scheme.

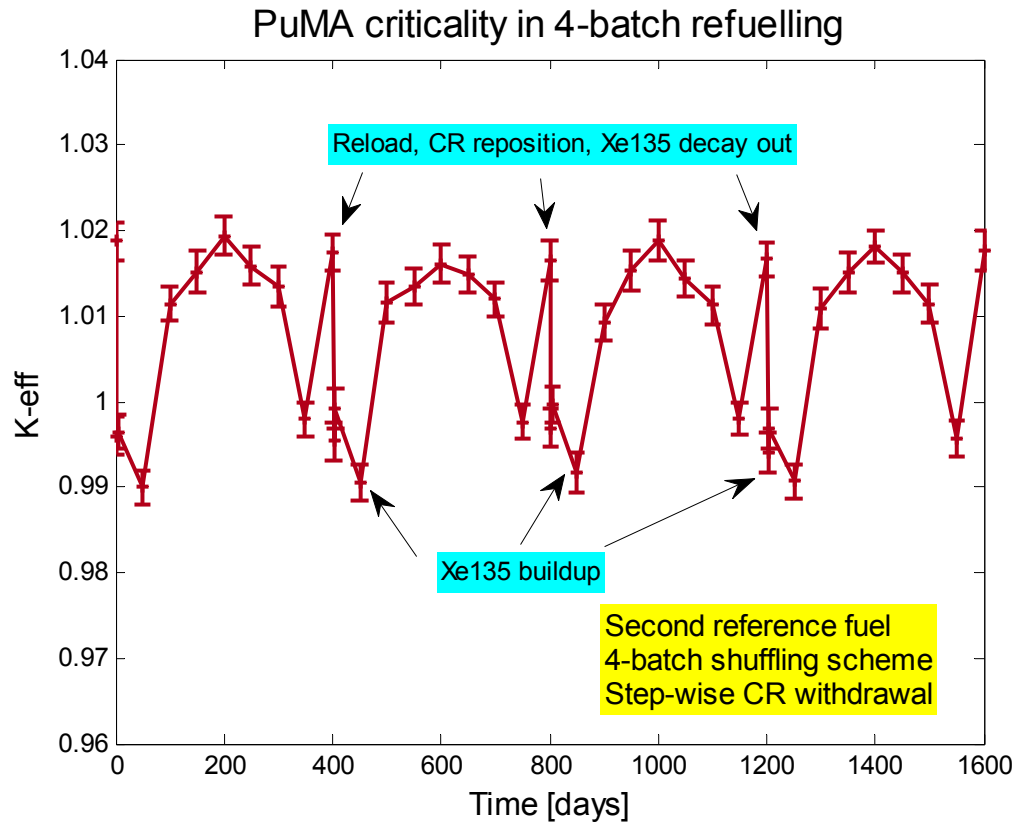

Figure 12. Criticality evolution with stepwise operation of CR.

5. Core characteristics in Pu/MA fuel cycle

5.1 Case identification and description

5.1.1. Origin: Jerzy Cetnar
5.1.2. Organisation: AGH
5.1.3. Case identifier: Pu-Cycle-D124-E12 (E12); MA-Cycle-D124-G1 (G1)
5.1.4. Date: 30.08.2009
5.1.5. Applied code system: MCB; see Chapter 2.

5.2 General fuel/reactor/system specifications

5.2.1. Main system dimensions: as D121 8-block-layers;
5.2.2. Coated particle dimensions: as D121
5.2.3. Initial coated particle composition: as D121
E12 - 2nd reference fuel;
G1 - 2nd reference fuel;
- see Table 1
5.2.4. Compact and block dimensions: as D121 8-block-layers
5.2.5. Number of compacts and blocks in the core: 4 393 728 compacts, 768 full fuel blocks, 384 fuel blocks with holes for CR/RCS, altogether 1152 fuel blocks
5.2.6. Fuel composition per nuclide: (outside coated particles; including impurities, burnable poison, etc.; units: $(barn\ cm)^{-1}$) – as D121, outside TRISO none
5.2.7. Block composition per nuclide (outside fuel compacts; including impurities, burnable poison, etc ; units: $(barn\ cm)^{-1}$) – as D121, no homogenization applied
5.2.8. Number of coated particles per compact: 9054
5.2.9. Operating cycle length (units: full power days) E12 – 420 ; G1 – 350;
5.2.10. Reload stop duration: 50 days
5.2.11. Nominal reactor power: 600 MWth
5.2.12. Capacity factor (units: %): 100%
5.2.13. Number of fuel batches: 4
5.2.14. Nominal coolant inlet temperature: 746.15 K
5.2.15. Nominal coolant inlet pressure : 7.067 MPa
5.2.16. Nominal coolant outlet temperature at nominal HFP conditions: 1124.75 K
5.2.17. Nominal coolant outlet pressure at nominal HFP conditions : 7.027 MPa
5.2.18. Nominal coolant mass flow: 320 kg/s
5.2.19. Control rod positions: see **Błąd! Nie można odnaleźć źródła odwołania.**.
5.2.20. Description of fuel cycle strategy and other relevant information on the specific case: see Chapter 3.

5.3 Rating and power density

See Chapter 4.2 and Annex

Table 7. Power density and ratings for case G1 (2nd fuel vector); for calculation of power density the volume of active core of 128.85 m^3 has been used.

Parameter	BOL 0 days	HFP 5 Days	Maximum 150 Days	MOL 175 days	EOL 350 Days
Power produced per compact [W]	136.56				
Maximum compact power [W]	282.54	280.76	647.15	504.45	494.07
Power produced per block [kW]	520.83				
Maximum block power [kW]	1077.60	1070.83	2468.23	1923.96	1884.38
Power density in the core [W/cm^3]	4.66				
Maximum power density [W/cm^3]	9.63	9.57	22.07	17.20	16.85

5.4 Core inventory

5.4.1.Amount of each of the heavy metal isotopes present in the core

Table 8. Amount of the heavy metal isotopes [g]; case E12 (1st fuel vector)

Actinides	BOC	EOC (420 fpd)
U234	427	671
U235	95.9	150
U236	57.5	88.9
U238	0.457	0.798
Np237	31.2	54.3
Np238	0	0.084
Np239	0.025	0.037
Pu238	35 102	31 950
Pu239	396 570	191 900
Pu240	249 270	175 730
Pu241	209 710	180 750
Pu242	138 960	155 920
Pu243	0	19.6
Pu244	3.88	5.86
Am241	10 041	15 135
Am242m	280	358
Am243	29 195	42 868
Cm242	1 873	2 377
Cm243	60.0	93.5
Cm244	14 517	23 860
Cm245	1 147	1 770
Cm246	184	404
Cm247	2.76	6.53
Cm248	0.206	0.585
Sum	1 087 528	824 113

Table 9. Amount of the heavy metal isotopes [g]; case G1 (2nd fuel vector);

Actinides	BOC	EOC (350 fpd)
U234	707	1121
U235	120.7	204.5
U236	54.8	83.8
U238	0.307	0.509
Np237	82 738	67 876
Np238	0	124.9
Np239	0	0.171
Pu238	68 209	75 648
Pu239	417 660	239 380
Pu240	267 910	206 040
Pu241	176 590	172 250
Pu242	105 320	121 520
Pu243	0	16.6
Pu244	2.56	3.99
Am241	33 126	26 095
Am242m	741	783
Am243	34 494	41 179
Cm242	4 133	5 953
Cm243	156	218
Cm244	14 879	23 645
Cm245	1 185	1 806
Cm246	178	372
Cm247	2.59	6.14
Cm248	0.184	0.497
Sum	1 208 207	984 327

5.4.2. Amount of each of the fission product isotopes present in the core

Table 10. Amount of the fission product isotopes [g]; case E12 (1st fuel vector)

F.P.	BOC	EOC (420 fpd)
Se79	34.4	50.7
Rb87	2 035	2 999
Sr90	4 674	6 808
Zr93	8 675	12 815
Nb95	477	513
Tc99	12 533	18 253
Pd107	5 869	8 835
Sn126	564	832
I129	4 120	6 047
Cs135	9 342	14 042
Cs137	19 713	28 976
Sm147	1 353	2 278
Sm151	303	354
Eu154	4 417	6 381

Table 11. Amount of the fission product isotopes [g]; case G1 (2nd fuel vector)

F.P.	BOC	EOC (350 fpd)
Se79	27.7	41.9
Rb87	1 613	2 444
Sr90	3 718	5 600
Zr93	6 822	10 364
Nb95	519	618
Tc99	10 018	14 296
Pd107	4 488	6 961
Sn126	446	677
I129	3 277	4 931
Cs135	6 975	10 589
Cs137	15 449	23 482
Sm147	979	1 612
Sm151	266	321
Eu154	3 610	5 368

5.4.3. Amount of possible extra nuclides, such as burnable poisons (units: kg) at BOL, MOL, EOL (different values if applicable)

Table 12. Amount of the burnable poison [kg]; case E12 (1st fuel vector)

BP	BOC	MOC	EOC (420 fpd)
Eu151	8.93	5.85	3.78

Table 13. Amount of the burnable poison [kg]; case G1 (2nd fuel vector)

BP	BOC	MOC	EOC (350 fpd)
Eu151	10.39	7.81	5.43

5.5 Fuel

Fuel (actinide) consumption, actinide and fission product production and discharge burnup at nominal conditions. This includes extra nuclides, such as burnable poison:

5.5.1. Amount and composition of fresh fuel loaded into the system for one operating cycle, preferably per fuel type

5.5.2. Amount and composition of fuel discharged from (and not reloaded into) the system for one operating cycle, preferably per fuel type (per heavy metal and fission product nuclide;

- Directly after final discharge from the reactor
- After 100 years of decay after final discharge from the reactor

Table 14. Fuel and burnable poison loaded, discharged and consumed in one operating 4-batch cycle [g], negative consumption indicates net production; E12 case (1st fuel vector)

Actinides	Load	Discharge (1680 fpd)	Consumption	After 100 years of decay
U234	0	244	-244.00	4491
U235	0	54	-54.10	95.97
U236	0	31	-31.40	339.4
U238	0	0	-0.34	8.42
Np237	0	23	-23.10	3642
Np238	0	0	-0.08	0
Np239	0	0	-0.01	0
Pu238	10 553	7 401	3 152	3 600
Pu239	219 412	14 742	204 670	14 860
Pu240	96 403	22 863	73 540	31 540
Pu241	53 498	24 538	28 960	200
Pu242	27 625	44 585	-16 960	44 580
Pu243	0	20	-19.60	0
Pu244	0	2	-1.98	1.98
Am241	0	5 094	-5 094	25 760
Am242m	0	78	-78.00	49.44
Am243	0	13 673	-13 673	13 560
Cm242	0	504	-504	0.12
Cm243	0	34	-33.50	2.94
Cm244	0	9 343	-9 343	203
Cm245	0	623	-623	618
Cm246	0	220	-220	217
Cm247	0	4	-3.77	3.77
Cm248	0	0	-0.38	0.38
All actinides	**407 450**	**144 035**	**263 415**	**143 773**
Se79	0	16.3	-16.3	16.3
Rb87	0	964	-964	964
Sr90	0	2 134	-2 134	197
Zr93	0	4 140	-4 140	4 143
Nb95	0	36	-36	0
Tc99	0	5 720	-5 720	5 745
Pd107	0	2 966	-2 966	2 966
Sn126	0	268	-268	268
I129	0	1 927	-1 927	1 941
Cs135	0	4 700	-4 700	4 706
Cs137	0	9 263	-9 263	919
Sm147	0	925	-925	3 104
Sm151	0	51	-51	23.9
Eu154	0	1 964	-1 964	0.75
Selected F.P.	0	35 074	-35 074	24 994
Eu151 (BP)	5 228	85	5 143	85

Table 15. Fuel and burnable poison loaded and discharged per one operating cycle [g]; case G1 (2nd fuel vector);

Actinides	Load	Discharge (1400 fpd)	Consumption	After 100 years of decay
U234	0	414.00	-414.00	11 790
U235	0	83.80	-83.80	150.2
U236	0	29.00	-29.00	425.7
U238	0	0.20	-0.20	6.76
Np237	27 707	12 844	14 862	17 180
Np238	0	124.9	-124.9	0
Np239	0	0.17	-0.17	0
Pu238	11 816	19 255	-7 439	9 634
Pu239	201 688	23 408	178 280	23 510
Pu240	93 714	31 844	61 870	39 870
Pu241	35 856	31 516	4 340	257
Pu242	19 965	36 165	-16 200	36 170
Pu243	0	16.60	-16.60	0
Pu244	0	1.43	-1.43	1.43
Am241	11 409	4 378	7 031	31 240
Am242m	81	123.5	-42.00	78.27
Am243	5 704	12 389	-6 685	12 290
Cm242	0	1820	-1820	0.19
Cm243	0	62.00	-62.00	5.45
Cm244	0	8 766	-8 766	190
Cm245	0	621.0	-621	616
Cm246	0	194.0	-194	191
Cm247	0	3.55	-3.55	3.55
Cm248	0	0.31	-0.31	0.31
All actinides	**407 450**	**184 059**	**223 880**	**183 610**
Se79	0	14.2	-14.2	14.19
Rb87	0	831	-831	831
Sr90	0	1882	-1882	174
Zr93	0	3542	-3542	3544
Nb95	0	2230	-2230	0
Tc99	0	4278	-4278	4297
Pd107	0	2473	-2473	2473
Sn126	0	231	-231	231
I129	0	1654	-1654	1666
Cs135	0	3614	-3614	3619
Cs137	0	8033	-8033	797
Sm147	0	633	-633	2124
Sm151	0	55	-55	25.8
Eu154	0	1758	-1758	0.67
Selected F.P.	0	31 228	31 228	19 796
Eu151 (BP)	5 228	267	4 960	267

5.5.3.Attained discharge burn-up of the fuel (units: MWd/kg).

Case G1:

- Minimum value 425.0
- Average value 506.3
- Maximum value 575.6
- Average FIMA: 55%

Case E12:

- Minimum value 576.0
- Average value 642.7
- Maximum value 694.0
- Average FIMA 65%

The quoted numbers concern burnup on zone level (1/6 of one block row and layer). The differences on smaller scale are estimated below 2%.
See Chapter 4.2.3.

5.6 Temperatures at nominal conditions

5.5.4. Coated particle temperature (units: K):

- Maximum value occurring anywhere in the core at BOL, MOL, EOL (different values if applicable)
- Maximum value occurring anywhere in the core at any time during the operating cycle

5.5.5. Block surface temperature (units: K):

- Maximum value occurring anywhere in the core at BOL, MOL, EOL
- Maximum value occurring anywhere in the core at any time during the operating cycle

Results for case G1:

Table 16. Maximum temperature [K] in 4-batch 350-day cycle with 2nd reference

Element	BOL 0 days	Maximum 150 Days	MOL 175 days	EOL 350 Days
Coated particle	1296	1461	1335	1349
Block surface	1128	1274	1237	1273

5.7 Temperature reactivity coefficients

The temperature reactivity Doppler constant coefficient α_T is subsequently calculated as shown in equations 19, 20 and 21 below. In case of LWR reactors with uranium or mixed uranium plutonium oxide fuel, the Doppler constant D (for the fuel)

$$\alpha_T = \frac{d\rho}{dT} \tag{19}$$

$$D = T \cdot \frac{d\rho}{dT} \approx \frac{\rho_{DELTA} - \rho_{REF}}{\ln(\frac{T_{DELTA}}{T_{REF}})} = \frac{\frac{1}{k_{REF}} - \frac{1}{k_{DELTA}}}{\ln(\frac{T_{DELTA}}{T_{REF}})} \tag{20}$$

$$\alpha_T = \frac{D}{T} \tag{21}$$

is independent of temperature. However, that is not granted in HTR cores. In Table 17 below presented are results of reactivity coefficient assessment obtained with JEFF3.1 library in BOC with all control rods out. In Cold Zero Power (CZP), zero xenon conditions the reactivity change is calculated for 300K and 400K, whereas in Hot Zero Power (HZP) and Hot Full Power (HFP) – for 1000K and 1200K. Uncertainties of the summary results are about 5% for CZP and 3% for HZP and HFP.

Table 17. Reactivity coefficients at BOC in 4-batch 350-day cycle; 2nd reference fuel

Varied core element/state	D [pcm]	α_T [pcm/K]
Fuel /CZP	-1010	-2.905
Moderator /CZP	200	0.574
Reflector /CZP	720	2.073
Sum /CZP	**-90**	**-0.258**
Fuel /HZP	-2250	-2.050
Moderator /HZP	-7630	-6.952
Reflector /HZP	180	0.163
Sum /HZP	**-9700**	**-8.839**
Fuel /HFP	-2515	-2.294
Moderator / HFP	-6820	-6.215
Reflector / HFP	55	0.048
Sum /HFP	**-9280**	**-8.461**

5.6.1. Calculated at BOC with the start-up CR being withdrawn while the operational CR being inserted, the differences in reactivity between:

- CZP (zero xenon) state and HZP (zero xenon) state: -2020 [pcm]
- HZP (zero xenon) state and HFP (equilibrium xenon) state: -2430 [pcm]
- CZP (zero xenon) state and HFP (equilibrium xenon) state: -4450 [pcm]

The uncertainties are about 3%.

5.8 Control rod worth

The *perturbed states* have "frozen" thermal hydraulics and the same nuclide concentrations as the *reference state* anywhere in the system. The following items have been calculated at BOL:

5.8.1. Control rod worth at CZP:

- All Start-up CR worth: 8 200 [pcm]
- All Operational CR worth: 6 300 [pcm]
- All CR worth: 14 500 [pcm]

5.8.2. Control rod worth at HZP

- All Start-up CR worth: 8 410 [pcm]
- All Operational CR worth: 6 570 [pcm]
- All CR worth: 14 980 [pcm]

5.8.3. Control rod worth at HFP

- All Start-up CR worth: 8 390 [pcm]
- All Operational CR worth: 6 480 [pcm]
- All CR worth: 14 870 [pcm]

6. Conclusions

In the course of presented study, we have been investigating the physics of the PUMA core in the deep burn conditions using Monte Carlo methodology. Few novel features of Monte Carlo burnup modelling were applied in order to analyse the core features deeply. The most important findings are summarised below.

- Power profile peaking in the reflector vicinities need to be assessed in a finer radial mesh than the thickness of one block, in order to avoid power peaking underestimation.
- Power peaking can be controlled effectively with axial-only shuffling scheme, with additional power suppression in fresh fuel block by burnable poison.
- Operation of CR significantly influences axial distribution of power and burnup and reverses the effect of the temperature impact on the power profile.
- The modelling of CR operation is necessary for a proper evaluation of axial power profile and power peaks.
- Power peaks during fuel cycle occur when operational CR insertion level is raised above the block layer with fresh fuel.
- Statistical oscillations in Monte Carlo solution of transport equations in PUMA fuel cycle have been reduced by "bridge scheme" of burnup step.
- Temperature reactivity coefficients are negative in all conditions, but in CZP the graphite coefficient is positive, with no safety threat however.
- Achievable burnup of 65% FIMA for 1st reference fuel and 55% for 2nd reference fuel was found in our Monte Carlo model.

References

[1] X-5 Monte Carlo Team, “MCNP — A General Monte Carlo N-Particle Transport Code, Version 5”, LA-UR-03-1987, Los Alamos National Laboratory, 2003

[2] J. Cetnar “General solution of Bateman equations for nuclear transmutations” Annals of Nuclear Energy Volume: 33, Issue 7, May 2006, pp. 640-645

[3] J. Cetnar, W. Gudowski and J. Wallenius "MCB: A continuous energy Monte Carlo Burnup simulation code", In "Actinide and Fission Product Partitioning and Transmutation", EUR 18898 EN, OECD/NEA (1999) 523.

[4] J. Cetnar, et al. ”Reference Core Design for a European Gas Cooled Experimental ADS AccApp’03 Conference, San Diego June 2003, p. 772

[5] Firestone, R., B., et al.: ”Table of Isotopes, 8E” John Wiley & Sons, Inc.(1996)

[6] W. Pfeiffer et al. “POKE A Gas-Cooled Reactor Flow and Thermal Analysis Code” GA-10226 Gulf General Atomic Incorporated, 1970

[7] A. G. Croff: “A User’s Manual for the ORIGEN2 Computer Code”, ORNL /TM-7157 (Oct. 1980)

[8] J. Zakowa “MCNP/MCB analysis of GT-MHR” Deliverable D124, EU FP6 project PUMA

[9] J. Kuijper et al. ”Selected Reference HTGR Designs and Fuel Cycle Data” Deliverable D121 EU FP6 project PUMA

ANNEX: Auxiliary tables and figures

Table 18. Fuel kernel power density [kW/cm^3] after 5 full power days in 350-day equilibrium cycle with 2nd reference fuel.

	Row #4		Row #5		Row #6		Row #7		Row #8	
Layer #1	0.80	0.92	0.98	1.09	0.77	0.58	0.47	0.49	0.29	0.17
	1.19	0.90	1.06	1.00	1.06	0.76	0.75	0.65	0.53	0.29
	1.38	1.48	1.39	1.36	1.34	1.16	1.14	1.17	0.75	0.60
Layer #2	3.43	2.31	3.47	3.86	3.79	3.26	2.89	2.67	2.08	2.07
	3.41	3.25	4.30	4.80	4.57	4.11	3.23	2.89	2.55	3.20
	4.41	4.21	4.68	4.55	5.05	4.74	4.22	3.70	3.37	3.52
Layer #3	3.00	3.29	3.29	4.30	4.33	3.73	3.31	2.96	2.88	2.61
	2.91	2.95	3.59	3.98	3.69	4.77	3.07	3.32	3.02	2.64
	3.60	3.80	3.84	3.67	4.51	4.41	3.26	3.04	3.03	2.87
Layer #4	4.72	4.35	4.34	5.14	5.87	4.79	3.96	3.59	3.24	2.90
	4.51	4.16	5.05	4.97	5.79	4.91	3.91	3.87	3.59	3.34
	4.84	4.09	5.07	5.56	5.54	5.07	4.77	4.43	3.80	3.59
Layer #5	6.08	5.89	4.94	6.11	6.68	6.49	4.60	4.98	4.45	4.28
	5.09	4.67	5.27	6.24	5.50	5.52	4.59	3.40	3.66	3.97
	6.50	5.28	5.48	6.29	6.86	6.86	5.26	4.12	3.13	3.50
Layer #6	3.90	4.49	4.63	5.01	5.30	3.93	3.68	2.92	2.48	1.99
	3.57	3.33	4.79	5.19	5.15	5.08	3.74	3.54	2.86	2.06
	3.73	4.21	4.96	5.02	4.63	3.96	3.32	3.51	2.87	2.27
Layer #7	5.24	6.51	6.68	6.34	7.33	6.06	4.92	4.93	4.31	4.45
	5.13	4.86	6.08	5.15	5.33	5.52	4.25	3.85	3.31	3.58
	4.81	4.97	4.82	5.97	6.20	5.97	4.77	4.19	3.69	3.46
Layer #8	2.92	3.30	4.19	3.63	3.18	3.65	3.46	2.91	2.47	2.35
	2.42	2.89	2.97	2.78	3.16	2.73	2.70	2.19	1.58	1.40
	1.76	2.27	2.72	3.02	2.60	2.44	2.20	1.85	1.57	1.20

Table 19. Fuel kernel power density [kW/cm^3] after 150 full power days in 350-day equilibrium cycle with 2nd reference fuel.

	Row #4		Row #5		Row #6		Row #7		Row #8	
Layer #1	0.09	0.16	0.13	0.10	0.10	0.08	0.11	0.13	0.09	0.09
	0.22	0.20	0.32	0.22	0.19	0.18	0.16	0.14	0.16	0.12
	0.39	0.34	0.46	0.47	0.38	0.37	0.28	0.16	0.21	0.23
Layer #2	0.87	0.82	0.82	1.46	0.91	1.53	0.78	0.75	0.89	1.10
	1.87	1.37	1.40	1.42	1.50	1.07	0.95	0.85	0.91	0.84
	2.01	2.09	2.18	2.87	1.97	1.83	1.36	1.06	1.11	1.03
Layer #3	1.49	1.82	1.70	2.16	1.99	1.60	1.50	1.46	1.01	0.90
	1.47	1.79	1.82	2.20	2.10	1.93	1.44	1.42	1.46	0.99
	1.95	1.69	2.11	2.00	2.03	1.92	1.59	1.75	1.27	1.28
Layer #4	2.66	2.50	2.93	3.48	2.92	2.30	1.99	1.38	1.64	1.13
	2.56	2.53	2.81	2.44	2.12	2.35	1.96	1.52	1.50	1.16
	2.31	3.15	3.18	2.64	2.51	2.52	2.45	2.06	1.79	1.64
Layer #5	3.52	2.84	2.68	3.89	3.76	3.59	2.66	2.51	2.33	2.83
	2.74	3.02	3.28	3.99	3.88	3.47	3.35	3.17	2.36	2.97
	3.41	3.90	4.61	4.50	4.77	4.99	4.07	4.39	3.47	4.78
Layer #6	2.19	3.75	3.96	4.18	4.69	4.67	4.69	4.27	4.01	4.10
	3.16	3.45	4.31	4.81	5.15	5.59	6.31	5.58	5.57	5.18
	3.52	4.37	5.06	4.73	5.45	5.48	6.37	6.34	6.64	6.95
Layer #7	7.32	7.34	7.82	8.29	10.00	10.07	9.47	11.39	10.93	16.87
	7.47	6.92	7.70	8.84	8.62	9.02	9.61	10.85	10.63	14.84
	6.47	6.92	7.83	8.18	9.91	9.95	10.19	10.57	10.69	15.15
Layer #8	3.62	4.56	4.78	5.07	4.79	5.58	6.25	6.85	6.80	6.70
	2.24	3.19	2.93	3.57	4.30	4.65	4.64	4.75	4.83	5.15
	1.87	2.48	3.31	2.99	3.20	4.13	3.86	3.40	4.09	3.82

Table 20. Fuel kernel power density [kW/cm^3] after 350 full power days in 350-day equilibrium cycle with 2nd reference fuel.

	Row #4		Row #5		Row #6		Row #7		Row #8	
Layer #1	0.45	0.60	0.47	0.35	0.41	0.38	0.30	0.33	0.30	0.13
	0.30	0.49	0.48	0.53	0.50	0.40	0.47	0.36	0.33	0.20
	0.71	0.85	0.81	0.61	0.54	0.48	0.54	0.56	0.55	0.32
Layer #2	1.98	1.49	1.78	1.67	1.99	1.55	1.55	1.25	1.18	1.48
	2.34	2.64	2.05	2.14	2.27	2.05	2.07	1.67	1.53	1.58
	3.21	2.58	2.70	2.75	2.95	2.87	2.52	1.87	2.02	1.61
Layer #3	2.21	2.47	2.48	2.52	2.28	2.51	2.27	2.20	1.85	1.54
	2.54	2.93	2.98	3.41	2.76	2.38	2.43	2.38	2.10	2.09
	3.48	3.14	3.42	3.58	3.84	3.51	3.40	3.72	2.75	2.65
Layer #4	3.88	4.00	4.69	4.49	4.84	4.76	5.57	5.55	4.78	5.33
	4.79	4.97	5.32	5.13	5.99	6.36	6.14	6.15	6.23	7.07
	3.95	4.65	5.30	5.60	6.32	7.05	7.80	8.29	8.07	9.84
Layer #5	4.45	6.14	6.18	7.63	8.10	8.94	9.50	9.19	9.38	12.88
	5.83	5.14	5.56	7.03	8.20	8.31	7.81	8.38	7.63	11.01
	5.86	4.43	6.02	6.63	8.11	7.46	7.44	7.40	7.05	9.29
Layer #6	3.15	3.78	4.21	4.31	4.62	4.43	4.95	4.99	5.12	4.82
	2.98	3.21	3.30	3.72	3.88	4.16	4.41	4.84	4.38	4.35
	2.50	2.97	2.71	2.73	3.02	3.35	3.42	3.73	3.61	3.22
Layer #7	3.98	3.30	3.33	4.02	3.99	5.29	4.68	4.57	4.59	5.79
	3.38	3.03	2.73	3.97	3.52	3.64	3.89	3.83	3.61	5.15
	2.87	2.25	3.51	3.24	3.66	3.47	3.66	3.93	3.72	4.80
Layer #8	1.17	1.48	1.70	1.33	1.79	1.77	2.07	2.20	2.17	1.99
	1.12	0.90	0.96	1.16	1.11	1.37	1.98	1.44	1.47	1.24
	0.91	1.08	1.18	0.87	0.87	1.13	1.26	1.18	1.01	0.89

Table 21. Zone average fuel temperature [°C] after 5 full power days in 350-day equilibrium cycle with 2nd reference fuel.

	Row #4		Row #5		Row #6		Row #7		Row #8	
Layer #1	526.4	523.9	527.7	527.8	520.8	512.7	512.1	511.8	507.2	499.4
	539.5	535.6	537.2	535.2	532.0	523.5	525.0	525.2	517.4	508.2
	571.9	559.1	567.1	566.7	564.7	554.9	556.7	557.6	543.3	536.2
Layer #2	620.5	596.4	621.9	628.3	622.2	609.5	605.4	604.0	586.8	592.2
	661.8	641.1	670.9	676.7	672.1	659.8	650.6	644.6	632.1	650.9
	683.8	673.5	689.5	695.2	697.1	685.7	680.3	672.2	666.3	680.1
Layer #3	683.7	679.5	688.7	703.3	701.2	700.2	688.5	687.1	685.8	684.8
	690.9	688.7	699.6	709.9	707.3	723.2	694.2	701.5	703.0	696.5
	726.7	720.8	725.5	729.4	741.4	746.6	717.4	722.3	725.6	719.7
Layer #4	767.4	753.3	758.0	764.8	786.4	769.0	748.4	750.7	753.2	746.3
	796.4	773.2	792.0	796.5	813.9	794.3	780.5	785.7	785.3	779.1
	832.3	804.9	816.5	828.5	839.1	829.0	814.2	825.4	822.0	818.2
Layer #5	871.0	845.4	837.6	863.8	867.3	867.0	840.7	850.1	854.2	856.1
	901.9	868.3	864.5	893.2	890.7	897.0	867.8	856.7	865.4	878.1
	921.1	884.9	885.4	908.7	913.3	911.3	888.9	866.3	863.5	875.4
Layer #6	911.0	889.1	895.8	913.5	921.4	907.5	890.2	876.3	868.4	861.4
	905.5	890.1	912.7	925.8	924.1	913.4	893.7	894.5	886.6	865.5
	935.6	932.4	950.0	954.2	954.5	939.8	918.8	931.3	922.6	907.4
Layer #7	980.2	985.6	995.6	984.7	996.6	979.3	956.1	968.7	962.3	963.8
	1010.6	1003.1	1014.6	1004.7	1016.0	1012.6	984.4	988.7	984.0	991.3
	1012.0	1001.6	1009.4	1011.8	1013.9	1020.2	998.8	996.5	992.4	993.8
Layer #8	994.2	992.4	1000.5	995.9	994.6	1001.5	995.5	990.5	983.9	981.7
	979.6	983.3	991.0	982.5	982.3	982.8	984.7	979.3	970.4	964.9
	975.9	983.6	987.0	987.5	987.4	980.3	982.3	977.2	968.6	958.0

Table 22. Zone average fuel temperature [°C] after 150 full power days in 350-day equilibrium cycle with 2nd reference fuel.

	Row #4		Row #5		Row #6		Row #7		Row #8	
Layer #1	496.8	498.0	499.2	495.8	495.3	494.6	495.1	496.5	496.2	494.4
	502.6	502.0	505.4	501.9	500.1	499.2	498.3	497.7	498.5	496.2
	515.2	512.1	515.8	519.5	511.5	516.3	507.3	504.8	507.5	506.6
Layer #2	543.0	532.8	533.7	545.1	532.1	539.4	522.3	518.9	523.5	522.7
	578.9	563.2	562.2	575.0	557.6	554.5	538.0	531.7	536.3	530.9
	597.6	590.6	587.4	605.5	579.6	568.8	553.8	544.9	543.9	534.3
Layer #3	599.2	603.3	597.3	618.0	594.7	582.5	566.0	559.4	553.1	537.9
	608.8	609.7	607.8	621.6	606.1	594.8	574.7	572.0	565.0	544.7
	637.5	626.4	633.0	643.0	624.1	610.2	588.4	581.5	575.8	553.3
Layer #4	670.2	654.4	663.4	672.0	643.8	627.4	605.3	586.6	586.5	558.1
	688.7	684.3	687.6	682.6	652.8	643.9	622.2	598.2	597.3	566.0
	711.3	710.7	704.5	701.8	675.7	668.6	643.3	621.3	614.3	589.6
Layer #5	743.3	730.1	720.2	742.5	716.6	701.5	669.8	650.1	636.5	622.2
	766.0	757.3	756.2	778.5	754.9	737.7	704.2	689.5	663.1	659.2
	778.7	794.5	800.3	806.1	790.5	778.9	745.2	731.9	701.8	696.8
Layer #6	788.9	818.9	825.9	831.9	822.7	815.9	796.5	771.2	752.2	724.7
	817.9	842.8	855.9	861.9	855.6	851.3	854.3	821.2	814.5	767.5
	893.7	909.6	922.6	921.0	928.1	921.3	924.0	913.6	909.7	899.1
Layer #7	1003.2	1000.8	1008.8	1015.4	1026.9	1019.4	1011.7	1033.9	1024.6	1078.1
	1074.3	1059.5	1070.5	1087.0	1092.3	1086.9	1085.4	1109.4	1101.6	1172.2
	1073.1	1075.0	1085.6	1095.6	1103.0	1100.9	1108.5	1118.7	1117.2	1154.9
Layer #8	1031.3	1054.7	1052.8	1060.7	1063.3	1068.7	1076.6	1081.6	1081.7	1068.1
	997.0	1028.2	1022.7	1030.1	1031.2	1042.8	1042.0	1038.3	1044.5	1003.3
	986.4	1018.9	1022.0	1022.3	1030.9	1047.0	1034.6	1018.5	1034.9	990.2

Table 23. Zone average fuel temperature [°C] after 350 full power days in 350-day equilibrium cycle with 2nd reference fuel.

	Row #4		Row #5		Row #6		Row #7		Row #8	
Layer #1	496.9	591.4	580.3	609.6	592.8	609.0	603.4	609.8	624.3	607.0
	502.8	576.0	570.5	586.5	574.8	586.6	586.4	600.2	604.3	590.1
	515.8	563.4	560.3	565.8	558.5	563.1	569.7	588.0	581.8	569.3
Layer #2	544.3	561.9	557.5	560.5	551.8	553.0	559.9	572.6	568.2	553.1
	581.1	557.2	551.9	552.7	544.5	545.4	547.6	553.6	553.6	537.8
	600.5	559.3	553.3	551.9	545.1	544.0	546.1	550.1	550.6	533.8
Layer #3	602.4	576.9	574.5	568.5	563.8	557.7	560.9	563.0	563.6	548.0
	612.4	612.9	607.4	599.5	600.2	587.5	589.4	585.3	584.6	573.4
	641.9	653.5	639.8	632.9	634.9	621.7	619.9	607.1	607.7	590.8
Layer #4	652.3	677.3	666.7	658.2	655.9	648.0	640.7	625.3	626.6	597.4
	621.8	694.7	688.7	681.4	667.1	659.7	652.6	644.0	639.4	607.6
	604.3	721.4	716.7	712.2	692.9	676.5	673.1	673.1	658.0	628.4
Layer #5	629.4	756.9	760.7	748.7	741.2	719.8	724.1	728.0	701.8	674.0
	673.1	806.7	818.1	791.8	798.4	783.3	793.4	795.2	773.0	751.1
	716.4	856.6	869.2	838.2	854.7	850.8	860.3	863.7	855.7	844.1
Layer #6	744.6	902.7	913.2	896.0	914.8	920.3	936.8	942.1	941.6	953.7
	754.1	949.6	955.7	960.7	981.8	985.9	1000.0	1004.0	1001.6	1045.1
	777.5	970.9	989.8	999.0	1034.6	1021.5	1021.3	1028.9	1017.9	1070.4
Layer #7	823.7	972.0	1008.9	1001.6	1042.9	1014.2	1016.8	1022.9	1014.1	1037.8
	874.2	973.5	1001.8	982.7	1010.6	985.4	998.9	1004.8	1001.8	985.2
	915.4	976.8	987.5	967.0	985.8	972.1	985.6	998.2	991.7	956.7
Layer #8	941.3	989.9	993.5	974.4	991.8	991.5	994.9	1006.5	1001.4	972.0
	985.5	1010.8	1012.0	1004.8	1014.3	1022.4	1019.7	1024.2	1022.9	1015.2
	1045.4	1031.3	1030.5	1039.6	1038.9	1046.6	1044.9	1044.3	1042.7	1057.8

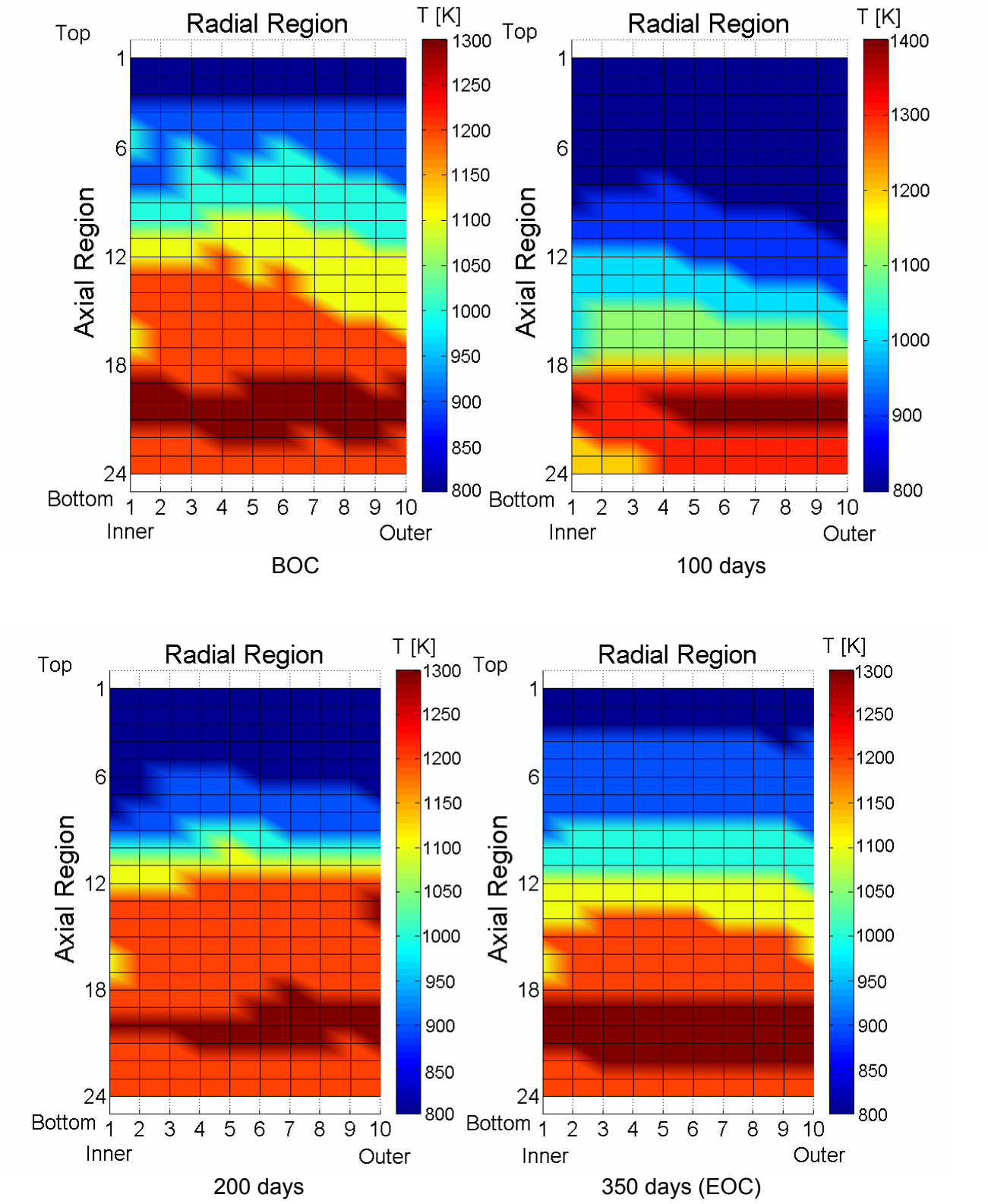

Figure 13. Temperature distribution with CR operation simulated stepwise; 350-day equilibrium cycle; 2nd reference fuel; CR-s shifted 100 cm every 50 days.